PVTx Measurements of Water−*n*-Pentane Mixtures in Critical and Supercritical Regions

Suleiman M. Rasulov[†] and Ilmutdin M. Abdulagatov*[,‡]

Institute of Physics of the Dagestan Scientific Center of the Russian Academy of Sciences, 367005 Makhachkala, M. Yaragskogo Str. 94, Dagestan, Russia, and Geothermal Research Institute of the Dagestan Scientific Center of the Russian Academy of Sciences, Makhachkala, 367030 Makhachkala, Shamilya Str. 39, Dagestan, Russia

The *PVTx* properties of H_2O + *n*-C_5H_{12} mixtures have been measured in the near- and supercritical regions. Measurements were made along 66 liquid and vapor isochores in the density range from (63 to 713) kg·m^{-3}, at temperatures from (303 to 684) K, and at pressures up to 63 MPa. Measurements were made for eight concentrations between 0.0270 and 0.8898 mole fractions of *n*-C_5H_{12}. The temperatures and pressures at the three-phase (liquid−liquid−gas) and two-phase (liquid−gas) boundary curves for the H_2O + *n*-C_5H_{12} mixtures were obtained using the isochoric (*P*−*T*) break point technique. The expanded uncertainty of the density, pressure, and temperature measurements at the 95 % confidence level with a coverage factor of $k = 2$ is estimated to be 0.12 % (at high densities) to 0.15 % (at low densities), (0.0005 to 0.03) MPa, and 15 mK, respectively. The critical property (P_C,T_C) data of the upper and lower branches of the critical curves were extracted from the derived phase-boundary data. The measured three-phase data were used to estimate the value of the upper critical end point. The value of the Krichevskii parameter was calculated from the direct measured *PVTx* and the derived critical property data.

Introduction

Water + hydrocarbon mixtures are very important in many scientific and technological aspects. Of practical relevance is the use of water flooding in enhanced crude oil recovery,[1] a procedure which is designed to maintain the reservoir pressure while oil is extracted through the oil well. Other applications for water + *n*-alkane mixtures are the hydrous pyrolysis of kerogen from shale oil, the hydrolysis of plastics, synthetic fibers, and polycarbonates for recycling,[2] the destruction of hazardous wastes, such as polychlorinated biphenyls,[3,4] and environmentally benign catalysis.[5] Binary aqueous *n*-alkane mixtures are an interesting case of mixing a strongly polar and a nonpolar component. For example, aqueous hydrocarbon mixtures show unusual critical line shapes. The critical curve of H_2O + *n*-C_5H_{12} is interrupted (no continuing critical curve between the pure components' critical points) and split into two branches, upper and lower. Water + *n*-alkane mixtures exhibit complex phase behavior, especially near the critical point of one of the components. Relatively few experimental critical locus data have been reported (see below) for aqueous *n*-C_5H_{12} solutions due to the high-pressure (over 22 MPa) apparatus needed. The difficulties in measuring the critical properties of aqueous solutions arise from several sources: (1) there are great differences between the critical properties of pure water and the pure *n*-C_5H_{12} (about 177 K and 19 MPa); (2) the apparatus has to be designed to tolerate high temperatures and high pressures in addition to the corrosion resistance of the vessel; and (3) the reliability of the calculated values is fair.

* To whom correspondence should be addressed. Present address: Thermophysical Properties Division, National Institute of Standards and Technology, 325 Broadway, Boulder, Colorado 80305. E-mail: ilmutdin@boulder.nist.gov.
[†] Institute of Physics of the Dagestan Scientific Center of the Russian Academy of Sciences.
[‡] Geothermal Research Institute of the Dagestan Scientific Center of the Russian Academy of Sciences.

Review of Available Experimental Data

Critical Properties of Binary Aqueous n-C_5H_{12} Solution. Aqueous solutions of less volatile, more strongly interacting molecules, such as *n*-alkanes, have critical curves that pass through a substantial temperature minimum before turning to high temperatures and pressures. The mutual solubility of hydrocarbons and water is very low, and the three-phase equilibrium line occurs at significantly higher pressures than the vapor-pressure curve of the pure alkanes. The liquid−gas critical curve that connects the critical end point of the three-phase line and the critical point of pure *n*-alkane is rather short, although for higher *n*-alkanes this critical line is very long. There is no continuous critical curve between the pure water and the pure hydrocarbon critical points (see Figure 1). One of the critical curves (lower critical curve) goes from the point T_C of the less volatile component (*n*-pentane) and terminates at the upper critical point liquid−liquid−gas (LLG) equilibrium end points (upper critical end point; UCEP, see Figure 2). The other critical curve (upper critical curve), originating from the pure water critical point $T_C(H_2O) = 647.1$ K extends toward very high pressures and has a minimum with respect to temperature at the point ($T_{Cmin} = 624.5 \pm 0.5$ K and $P_{Cmin} = 34.2 \pm 0.5$ MPa), where the two-phase region separates into two parts (see also Figure 3). The shape of the critical curves for water + *n*-alkanes changes systematically from system to system.[6,7] It shifts to lower pressures with the *n*-alkane carbon number. The temperature at the critical locus minimum does not differ very much. The temperature at the critical end point is noticeably less than pure alkane's critical temperatures for the mixtures with butane and heavier alkanes. The critical curves of H_2O + *n*-alkane mixtures show typical gas−gas equilibria of the second

10.1021/je100073y
Published on Web 05/14/2010

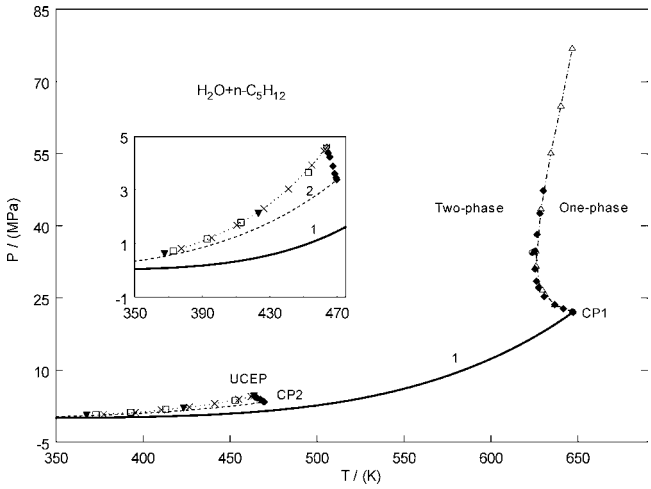

Figure 1. $P-T$ phase diagram and upper and lower critical lines of the $H_2O + n\text{-}C_5H_{12}$ mixture. 1, the vapor-pressure curve of pure water (IAPWS[26]); 2, the vapor-pressure curve of pure $n\text{-}C_5H_{12}$ (Span and Wagner[48]); CP1, critical point of pure water; CP2, critical point of pure $n\text{-}C_5H_{12}$; ◆, Brunner;[7] △, de Loos et al.;[6] ×, Brunner;[7] □, Jou and Mather;[17] ▼, Gillespie and Wilson;[18] ○, Connolly;[8] ····, three-phase (LLG) curve; UCEP, upper critical end point (this work).

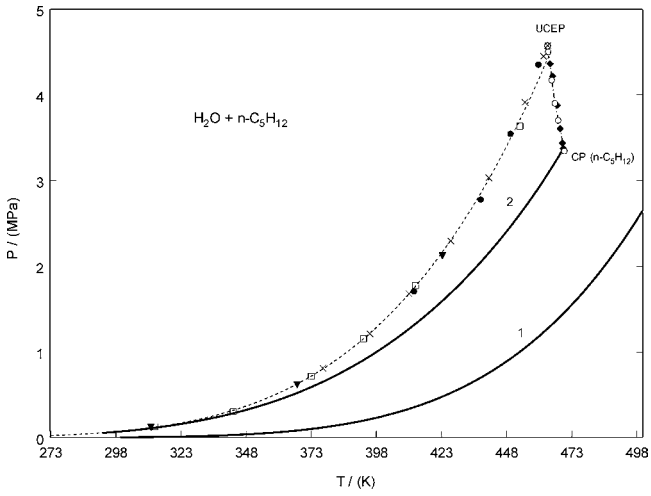

Figure 2. Measured three-phase (LLG) and lower critical curves for the $H_2O + n\text{-}C_5H_{12}$ mixture together with vapor-pressure curves for pure components. ●, this work; ◆, Brunner;[7] ×, Brunner;[7] □, Jou and Mather;[17] ▼, Gillespie and Wilson;[18] ○, this work; 1, the vapor-pressure curve of pure water (IAPWS[26]); 2, the vapor-pressure curve of pure $n\text{-}C_5H_{12}$ (Span and Wagner[48]); dashed line is calculated from the correlation.[17]

type.[6,7] The critical parameters for the water + *n*-pentane mixture has been also measured by Connolly[8] and Roof.[9] The critical point is defined by Connolly[8] as the minimum temperature for the mixing of two components in all proportions as a liquid or as the maximum temperature of a binary system for two liquid phases in equilibrium. The uncertainty in the critical measurement is 2 K and in the critical pressure is 1.01 MPa. Roof[9] reported the pressure and temperature of the three-phase critical point for 16 binary water + hydrocarbon mixtures. Measurements were made using the 15 in. Vycor glass capillary. The capillary was sealed off at the top and connected at the bottom to a mercury pump and a pressure gauge. The steel ball was moved slowly up and down in the capillary to achieve equilibrium compositions. The disappearance of the interface into an opalescent hazy zone was chosen as the critical state. Measured values of the three-phase critical point for $H_2O + n\text{-}C_5H_{12}$ mixture are 463.71 K and 4.537 MPa. The critical parameters of the $H_2O + n\text{-}C_5H_{12}$ mixture were determined by

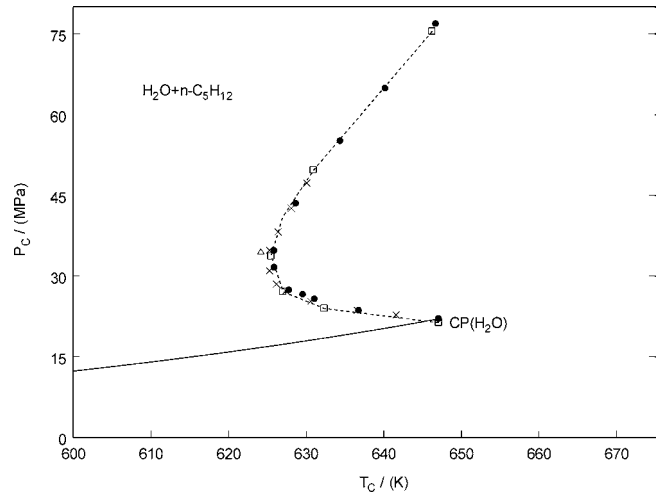

Figure 3. P_C-T_C projection of the upper critical curve of the $H_2O + n\text{-}C_5H_{12}$ mixtures reported by various authors together with the present data. ●, de Loos et al.;[6] △, Connolly;[8] ×, Brunner;[7] □, this work; solid line is the vapor pressure of pure water IAPWS;[26] ---, smoothed experimental curve.

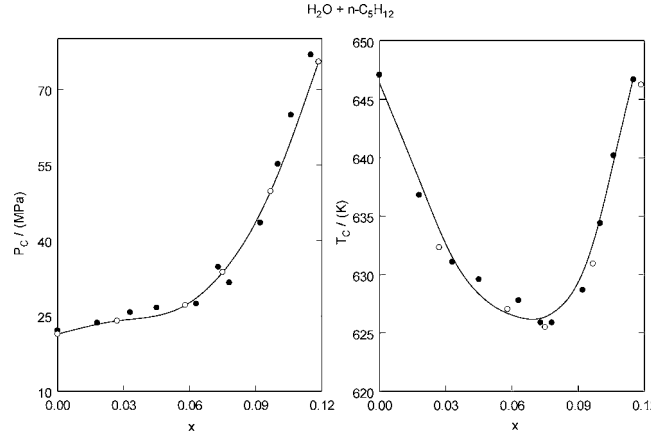

Figure 4. T_C-x and P_C-x projections of the upper critical curves of the $H_2O + n\text{-}C_5H_{12}$ mixture reported by de Loos et al.[6] together with the present data. ●, de Loos et al.;[6] ○, this work; —, smoothed experimental curve.

observing the behavior of the meniscus by de Loos et al.[6] As one can see from Figure 4 (right) in the T_C-x projection, the upper critical curve of the $H_2O + n\text{-}C_5H_{12}$ mixture observed a minimum at a concentration around 0.075 mole fraction of *n*-pentane, where $(dT_C/dx) = 0$. The P_C-x projection (Figure 4, left) of the critical curve shows no minimum (monotonically increasing with concentration). At low concentrations (up to 0.075 mole fractions) P_C weekly changes with x, while at concentrations above 0.075 the P_C-x curve is very steep. It is very important, because according to the isomorphism principle,[10,11] the near-critical behavior of binary fluids (C_V and other thermodynamic properties) is controlled by two characteristic parameters, K_1 and K_2,[10] that are determined by the slopes of the critical curves (T_C-x and P_C-x). The parameter K_1 controls strongly divergent properties such as the isothermal compressibility K_T and the isobaric heat capacity C_P. The parameter K_2 is responsible for the deformation of the weak divergence of C_V and defines the range of Fisher renormalization[11] of the critical exponent α. The isochoric heat capacity behavior of a binary mixture will exhibit the same behavior as those of the pure components in the range of temperature $\tau \gg \tau_2$,[10] where

$$\tau_2 = \left[A_0^+ \frac{K_2^{\,2}}{x(1-x)}\right]^{1/\alpha} \qquad \Delta\rho_2 = B_0 \tau_2^{\beta}$$
$$K_2 = \frac{x(1-x)}{T_C(x)} \frac{dT_C}{dx} \qquad \tau = \frac{T - T_C}{T} \qquad \Delta\rho = \frac{\rho - \rho_C}{\rho_C} \tag{1}$$

Therefore, at concentrations of 0.075 mole fraction of *n*-pentane, where $(dT_C/dx) = 0$, the value of $K_2 = 0$, and the characteristic reduced temperature τ_2 is zero. Thus, the condition $\tau \gg \tau_2$ is valid at any temperatures along the critical isochore for the composition $x = 0.075$ mole fraction of *n*-pentane. This is means that the binary mixture H_2O + *n*-C_5H_{12} with concentrations of $x = 0.075$ mole fraction of *n*-pentane behave near the critical point as pure fluid ($C_V \propto \tau^{-\alpha}$). At any other concentrations where the condition $\tau < \tau_2$ is valid, those properties that diverge weakly in single-component fluids will be saturated, and all critical exponents will be renormalized by a factor $1/(1 - \alpha)$($C_{VX} \propto \tau^{\alpha/(1-\alpha)}$).

The P_C-T_C projections of the critical curves for 23 binary mixtures of water + *n*-alkanes with *n*-alkane carbon numbers $i = 1$ to 12 and $i = 14$, 16, 18, 20, 24, 25, 26, 28, 30, 32, and 36 were measured by Brunner.[7] He showed that all of the critical curves are interrupted and its shape changes systematically with *i*. Measurements were performed in a 30 cm^3 cylindrical high-pressure optical cell. The operating pressure of the cell is 200 MPa at 750 K. The uncertainties of pressure and temperature measurements at phase-boundary appearance or disappearance are 0.1 % and 0.2 K, respectively. The total uncertainty of the position of the critical pressure measurements is estimated to be 0.4 %. The LLG curves for these mixtures are at higher pressures than the vapor pressures of the pure components (see Figures 1 and 2) and end in an liquid−gas (LG) UCEP. The UCEP for the H_2O + *n*-C_5H_{12} mixture found by Brunner[7] is 463.8 K and 4.577 MPa. Our results (see below) for the UCEP are $x = 0.791$ mole fraction of *n*-pentane, $T_{UCEP} = 463.85$ K, and $P_{UCEP} = 4.575$ MPa. The temperature minimum of the critical curve for H_2O + *n*-pentane reported by de Loos et al.[12] is $T_{Cmin} = 624$ K and $P_{Cmin} = 34.4$ MPa. Our results (see below) are $T_{Cmin} = 625$ K and $P_{Cmin} = 34.0$ MPa.

Neichel and Franck[13] calculated the critical curves for water + *n*-alkane (C_1 to C_6 and C_{12}) mixtures at temperatures up to 670 K and at pressures up to 200 MPa using the perturbation-type equation of state with a repulsion and an attraction term with square-well potential for intermolecular interaction. The three adjustable parameters of the model (k_σ, k_ε, w_{ij}) have been calculated using the critical lines data (P_C, T_C, x_C).

PVTx Measurements. The largest gap in the database is found to be the thermodynamic properties measurements in the near- and supercritical regions for the H_2O + *n*-C_5H_{12} mixture. Most of the reported *PVTx* data cover the temperature and pressure ranges below the critical point. Almost all previous reported data are *PTx* (VLE data), not *PVTx*. They are not provided with density measurements. Here we will briefly review only work with *PVTx* and phase-boundary properties data at high temperatures and high pressures. *PVTx* properties of the H_2O + *n*-C_5H_{12} mixture in the supercritical region have been reported by Abdulagatov et al.[14,15] They used a constant-volume piezometer technique to measure *PVTx* relations at a fixed temperature of 647.05 K (close to the critical temperature of pure water) in the pressure range from (4 to 41) MPa and at concentrations from (0.028 to 0.694) mole fraction of *n*-pentane. The uncertainty of the density measurements was 0.5 % and pressure 2 kPa. de Loos et al.[6] reported phase-boundary curves (*PTx*) between the two- and one-phase regions for 12 compositions in the temperature range from (600 to 675) K and at pressures from (15 to 170) MPa. The uncertainty in the temperature, pressure, and concentration measurements was 0.1 K, 0.02 MPa, and 0.002 mole fraction, respectively. They found a second type of gas + gas equilibrium shape of the ($P-T$) isopleths. Brunner[7] measured the $P-T$ projection of the critical curves and LLG three-phase curve data for 23 binary mixtures of water + *n*-alkane. Connolly[8] measured the solubility (*PTx*) of *n*-pentane in near-critical water as a function of pressure at several constant temperatures from (573 to 625) K. The uncertainties in temperature and pressure measurements were within 0.02 K and 0.202 MPa, respectively. Scheffer[16] reported three-phase (LLG) curve data for the H_2O + *n*-C_5H_{12} mixture in the temperature range from (423 to 466) K. These data together with other published three-phase results are presented in Figure 2. Jou and Mather[17] measured three-phase equilibria in the H_2O + *n*-C_5H_{12} mixture over the range of temperature from (273 to 453) K using a visual cell. The uncertainty in temperature and pressure measurements was 0.1 K and 0.1 %, respectively. The results were fitted to Clausius−Clapeyron type equation. Three-phase equilibrium data for the H_2O + *n*-C_5H_{12} mixture were reported also by Gillespie and Wilson[18] in the temperature range from (311.5 to 423.3) K. Other properties such as excess enthalpy at high temperatures, from (363 to 698) K, were reported by Wormald et al.[19] Measurements were made using two flow calorimeters of different design for low and high pressures. In our previous publication[20] we reported preliminary *PVTx* data for this mixture for only one (0.075 mole fraction of *n*-pentane) composition at the temperature range from (303 to 684) K and at pressures up to 60 MPa. In this work we slightly modified the construction of the piezometer to improve the accuracy of the pressure measurements and temperature control. In particular, we replaced the diaphragm-type null indicator to a more sensitive one and used additional heating elements to improve the temperature control to accurately maintain the homogeneity of the temperature distribution along the length of piezometric tube. Therefore, the present data for the pressures systematically differ from the previous[20] measurements by (15 to 20) %. Thus, the primary objective of this work was to expand the existing *PVTx* database for the H_2O + *n*-C_5H_{12} mixture to higher temperatures (near- and above the critical temperature, up to 684 K) and pressures from (0.035 to 63.0) MPa.

Experimental Apparatus and Procedure

The high-temperature and high-pressure apparatus used for *PVTx* measurements of H_2O + *n*-C_5H_{12} is similar to that used in previous publications[20−25] to measure *PVTx* properties of pure 1-butanol, H_2O + *n*-C_5H_{12}, and H_2O + *n*-C_6H_{14} in the critical and supercritical regions. Detailed descriptions of the apparatus, the experimental procedure, and an uncertainty assessment have been described in our previous publications.[20−25] The measurements were made using the constant-volume method. The apparatus used for the present (P,V,T,x) measurements is schematically shown in Figure 5. The main part of the apparatus consisted of a piezometer (1), the system for the temperature control (7), the system for the filling piezometer with the sample, and the system for the pressure measurements. The most essential part of the apparatus is piezometrical tube. The cylindrical tube piezometer was made from stainless steel (12 × 18H10T, 12 chrome-18 nickel-10 titanium) with inner diameters of 8.721 ± 0.003 mm and outer diameters of 14.121 ± 0.003 mm. A diaphragm-type null indicator (2) (see Figure 5) was mounted on one of the ends of the piezometer, and a stop valve was mounted on the other end of the piezometer.

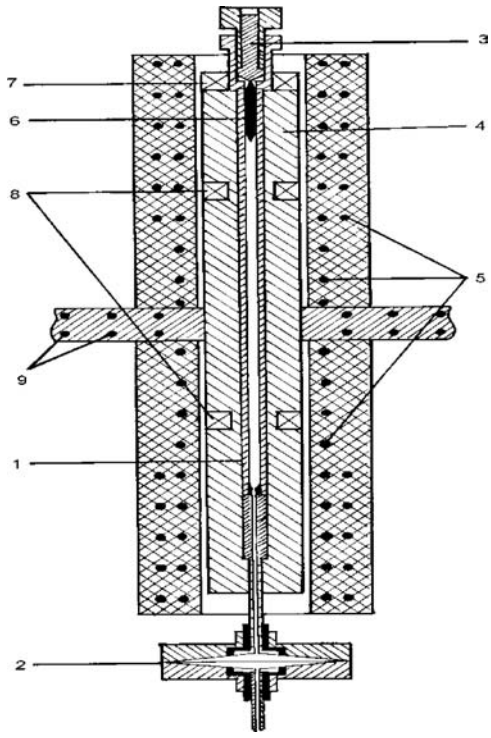

Figure 5. Schematic representation of the high-pressure and high-temperature apparatus for *PVTx* measurements: 1, body of the piezometer tube; 2, body of the diaphragm-type null indicator; 3, stop valve; 4, solid copper block; 5, three-sectioned heater; 6, stirrer (cylindrical form with conic end); 7, inductance coil to hold the stirrer; 8, coil for fixing the falling time of falling-body; 9, compensation heater.

The stop valve was used also to fill the piezometer with the fluid sample. The sample is intensely mixed using a stirrer (6) (cylindrical form with conic end) made from stainless steel. Stirring of the mixture was accomplished with the aid of a stirrer (6) that was moved by the turning the piezometer by an angle of 180° around the vertical axis. The thermostat was a massive, solid copper block (4) which was mounted on the piezometric tube to maintain the homogeneity of the temperature distribution along the length of piezometric tube. A three-section heating element was mounted on the surface of a solid cooper block to control the temperature in the thermostat. Cylindrical wells were used for a thermocouples and resistance thermometer (PRT) on the ends and on the middle of solid cooper block. The temperature difference between various sections of the cooper block was within 0.02 K.

Pressure was measured with a diaphragm-type null indicator (2). The diaphragm (40 mm in diameter and 0.05 mm thick) was made from 321 stainless steel. The membrane was compressed (squeezed) between the piezometer body and the null-indicator body with bolts (8) (see Figure 5). At the neutral point (position) the membrane touched the surface of the cylinder (4), and the distance between the membrane and the electrical contact (5) is about (0.2 to 0.3) mm. A basic part of the diaphragm-type null indicator (2) is membrane which was made of stainless steel (0.08 mm thick and 32 mm in diameter). The membrane is separated by the sample under study, and the pressure transmitted the liquid (castor oil) of the manometer.

System of Temperature Measurement and the Temperature Control. The main heater created the desired temperature using the high-precision temperature regulator (HPTR-3). The temperature homogeneity along the piezometer was controlled with two HPTR-3, differential thermocouples, and heaters. The temperature of the piezometer was measured with a platinum resistance thermometer (PRT-10) which was calibrated against a standard thermometer of the VNIIFTRI (Moscow). All temperatures were recorded on ITS-90. The uncertainty in temperature control and temperature measurements is within 20 mK and 15 mK, respectively.

The pressure of the sample (mixture) was measured with a dead-weight pressure gauge MP-600. The absolute sample pressure was calculated as

$$P = P_m + P_b + P_h \qquad (2)$$

where P_m is the pressure reading by the dead-weight pressure gauge (MP-600), P_b is the barometric pressure, and P_h is the pressure created due to the difference in oil levels in the manometer and null indicator. At low pressures (up to 1 MPa) the pressure in the piezometer was measured with a null indicator and standard manometer. At high pressures the pressure measurements were performed with the dead-weight pressure gauge MP-600. The values of P_h were calculated as $P_h = \rho_{oil} g \Delta h_m$ ($\Delta h_m = 0.45$ m), and the values of ρ_{oil} in the experimental conditions change from (760 to 1000) kg·m^{-3}. Therefore, the values of the P_h were changed within (0.0042 to 0.0044) MPa. The maximum uncertainty in the pressure measurements are within 0.0005 MPa at low pressures (below 1 MPa) and 0.03 MPa at high pressures. The sensitivity of the null indicator is within 0.005 MPa.

Since the inner volume V_{TP} of the piezometer is subjected to the effects of both temperature T and pressure P, it is essential to make appropriate corrections for these influences. The inner volume of the piezometer was calculated by taking into consideration corrections of the elastic pressure deformation and thermal expansion. The internal volume of the piezometer was previously calibrated by filling it with pure water. The volume of the piezometer $V_{T_0P_0} = m(H_2O)/\rho(H_2O)$ at room temperature $T_0 = 293.15$ K and at atmospheric pressure $P_0 = 0.1$ MPa was calculated from the well-established (IAPWS formulation, Wagner and Pruss[26]) density $\rho(H_2O)$ and mass of the water $m(H_2O)$. The uncertainty in the density of pure water at this condition is less than $\delta\rho < 0.001$ %. The derived value of volume at these conditions was $V_{T_0P_0} = (22.035 \pm 0.025)$ cm^3. It is necessary to know the volume of the piezometer, V_{PT}, at a given temperature T and pressure P, for the purpose of calculating densities $\rho(T,P) = m/V_{PT}$. Variations of the piezometer volume V_{PT} with temperature T and pressure P were calculated using the thermal expansion coefficient of the piezometer material, $\alpha = (16 \cdot 10^{-6}$ to $17.5 \cdot 10^{-6})$ K^{-1} in the temperature range from (273 to 673) K, and the pressure expansion coefficient of the piezometer, $\beta = 4 \cdot 10^{-5}$ MPa^{-1}.

$$V_{pT} = V_{p_0T_0}[1 + 3\alpha(T - T_0) + \beta(P - P_0)] \qquad (3)$$

The uncertainty in α and β is negligibly small (about 5 %) and did not affect to the density determination. For example, even a 20 % uncertainty in α and β causes less than 0.15 % uncertainty in the piezometer volume.

All masses were determined with an uncertainty of $5 \cdot 10^{-4}$ g. The volume of the piezometer at a given temperature T and pressure P was measured with an uncertainty of 0.011 %. The present experimental apparatus had negligible noxious volumes. To avoid the additional uncertainty in the density measurements which were introduced by the noxious volume, a diaphragm-type null indicator was mounted on one of the ends of the piezometer (see Figure 5). Taking into account the uncertainties of measurements of temperature and pressure, the combined expanded ($k = 2$) uncertainty of measuring the density was estimated to be 0.15 % at low densities and 0.12 % at high

Table 1. Comparisons between the Test Measurements and the Calculated Values of the Pressure of Pure Water along the Isochore of 351.1 kg·m^{-3}

T_s/K	P_{exp}/MPa (this work)	P_{cal}/MPa (IAPWS[26])	deviation/%
345.21	0.034	0.034	0.3
424.56	0.493	0.494	0.2
460.99	1.200	1.197	−0.2
500.19	2.646	2.649	0.1
538.06	5.081	5.078	−0.1
554.69	6.572	6.567	−0.1
599.35	12.252	12.241	−0.1
617.35	15.401	15.387	−0.1
625.16	16.953	16.941	−0.1
661.30	26.300	26.259	−0.2
677.22	31.034	31.110	0.2

densities. To check the reproducibility of the experimental density values, some of the measurements at selected temperatures and pressures were repeated at a few (5 to 6) times. The reproducibility of the data corresponding to repeated (P,T) is better than ± 0.1 %. To test the apparatus and procedures of the measurements and confirm the accuracy of the measurements, before engaging in measurements on the H_2O + n-C_5H_{12} mixture, the density of triple-distilled water was measured and compared with values calculated from IAPWS formulation.[26] Table 1 provides the present experimental *PVT* data for pure water at a selected constant density of 351.1 kg·m^{-3} measured using the same experimental apparatus. As one can see from Table 1 (see also Figure 6), the agreement between test measurements for pure water and IAPWS[26] formulations is good, and the absolute average deviation is AAD = 0.16 % (deviation statistics are: AAD = 0.16 %; bias = −0.02 %; standard deviation = 0.19 %; standard error = 0.06 %; maximum deviation = 0.3 %). This acceptable agreement between the present data and the IAPWS[26] calculations for pure water in the critical and supercritical conditions confirms the reliability and high accuracy of the measurements for the H_2O + n-C_5H_{12} mixture and gives us an assurance that our instrument is functioning correctly. The H_2O + n-C_5H_{12} mixture was prepared by weighing. Distilled water was used, and this was mixed with analytical reagent grade n-C_5H_{12} with a mole fraction purity of 0.998. The uncertainty in concentration was 0.001 mole fraction.

Results and Discussion

Measurements of the *PVTx* relation of the H_2O + n-C_5H_{12} mixtures were performed along 66 liquid and vapor isochores from (63 to 713) kg·m^{-3} as a function of temperature in the range from (303 to 684) K at pressures up to 63 MPa. These regions include upper and lower branches of the critical lines, the LLG three-phase line, and liquid−gas, liquid−liquid, and gas−gas phase equilibrium curves. Most measurements were made in a range of temperature and pressure in the immediate vicinity of the phase transition and the critical points to precisely determine the phase boundary properties (T_S,P_S) and the critical parameters (T_C,P_C). Detailed measurements of the phase transition boundary were allowed to precisely determine (see below) the shape of the LLG and LG phase boundary curves near the critical points and accurately determine the critical parameters (T_C,P_C) and therefore construction of the complete *PVTx* phase diagram of the binary H_2O + n-C_5H_{12} mixture. The critical and phase transition points are the key parameter in the construction of the phase diagrams. The measured values of temperature, density, and pressure for the H_2O + n-C_5H_{12} mixtures are presented in Table 2. Some selected experimental results are shown in Figures 7 and 8 in the $P-T$ and $P-\rho$ projections for the fixed composition of 0.0967 mole fraction of n-pentane. Figures 7 shows the $P-T$ dependence along various selected liquid and vapor isochores. As one can see from Figure 7, each measured liquid and vapor $P-T$ isochore far from the critical region clearly exhibits the break points which are indicate the phase transition (LLG ⇒ LG ⇒ L or G) occurring in the system heated in a closed volume. In Figure 9 (left) the present data are depicted along the selected near-critical isotherm−isochore (almost critical isotherm−isochore of pure water, 647.05 K and 326.13 kg·m^{-3}) and at the selected isotherm (right) and concentration (647.05 K and 0.0967 mole fraction of n-pentane) together with the data reported by Abdulatagov et al.[14,15] The initial slope, $(\partial P/\partial x)^{\infty}_{T_C V_C}$, of the critical $P-x$ isotherm−isochore (Figure 9, left) is defined as the value [(139.03 ± 3) MPa] of the Krichevskii parameter (direct measurement of the Krichevskii parameter). This value is very close to the value of the Krichevskii parameter calculated from the critical properties data [(144.11 ± 5) MPa]; see below. As one can see from Figure 9, the agreement is good enough (within 0.2 % to 0.5 %). The detailed view of the various parts (ranges) of the measured liquid and vapor $P-T$ isochors showed that each isochore contains a few break points which correspond to various types of phase transition points. In this work the measured *PVTx* data were used to accurately determine the location of the phase boundary (LG and LLG) curves using the "break points" technique. The break $P-T$ curves are often found in the system water + n-alkanes.[27,28]

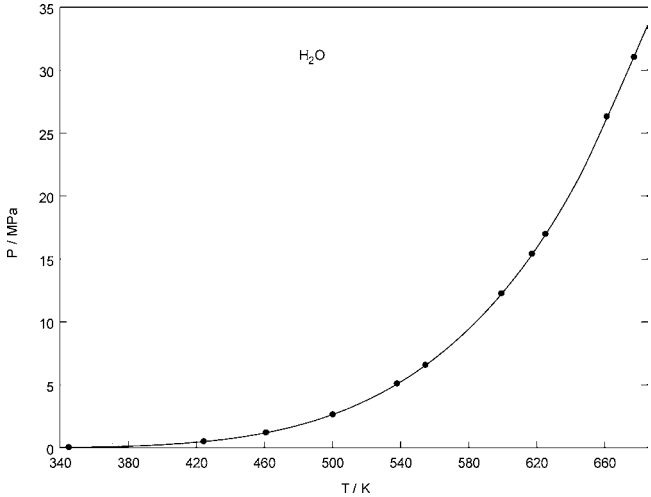

Figure 6. Comparison of the present measured values of pressure as a function of temperature along the selected isochore of 351.1 kg·m^{-3} for pure water with the values calculated from IAPWS[26] formulation.

Phase Boundary Parameter Determination. $P-T$ relations were measured for different fillings (liquid and vapor) of the piezometer. Breaks in the $P-T$ curves for mixtures of fixed overall concentration and density indicated the transition from a two- to a one-phase or from a three- to a two-phase region. This method was originally proposed by Lentz.[29] This technique was also successfully used to accurate determine the phase transition points for pure (Levelt Sengers and Hastings[30] and Bazaev et al.[31]) fluids and aqueous binary mixtures (Mather et al.,[27] Shmonov et al.,[28] Bach and Friedrichs,[32] Bazaev et al.,[33] and Polikhronidi et al.[34]). Each run for the *PVTx* measurements was normally started in the three-phase region and completed in the one-phase (liquid or vapor depending on filling factor) region. The present experimental *PVTx* data for the water−n-pentane mixture were used to extract the phase-boundary parameters (T_S, P_S) using a graphical−analytical technique for each measured isochore. The LLG and LG phase boundary data extracted from isochoric $P-T$ break points are presented in

Table 2. Experimental ($P\rho Tx$) Values of the H_2O + n-C_5H_{12} Mixtures

T/K	P/MPa	T/K	P/MPa	T/K	P/MPa	T/K	P/MPa	T/K	P/MPa	T/K	P/MPa
$x = 0.8898$ mole fraction of n-C_5H_{12}											
ρ/kg·m^{-3} = 63.30		ρ/kg·m^{-3} = 94.96		ρ/kg·m^{-3} = 126.60		ρ/kg·m^{-3} = 63.30		ρ/kg·m^{-3} = 94.96		ρ/kg·m^{-3} = 126.60	
309.89	0.047	310.80	0.049	310.51	0.0485	413.10	1.252	418.83	1.488	445.11	2.393
336.95	0.200	337.49	0.205	338.33	0.207	419.06	1.364	424.29	1.657	450.77	2.598
349.49	0.315	349.36	0.312	362.72	0.481	424.65	1.433	426.79	1.727	457.35	2.834
353.42	0.355	354.92	0.367	366.65	0.529	432.09	1.549	430.77	1.830	463.34	3.032
358.80	0.428	358.58	0.417	371.36	0.541	436.52	1.628	437.25	2.020	468.55	3.206
362.89	0.430	363.37	0.462	374.49	0.605	443.66	1.697	448.86	2.334	475.84	3.462
366.34	0.473	367.39	0.496	380.01	0.670	455.15	1.844	472.20	2.834	479.81	3.598
369.71	0.518	371.15	0.548	395.79	0.930	467.50	2.014	496.22	3.318	491.72	3.972
377.17	0.622	374.69	0.600	401.55	1.039	490.41	2.256	529.49	3.913	514.45	4.500
382.15	0.697	381.27	0.695	407.20	1.177	525.93	2.529	563.40	4.393	535.48	4.952
386.91	0.782	386.49	0.791	414.21	1.364	560.56	2.771	595.60	4.765	570.01	5.657
392.59	0.885	393.45	0.922	420.15	1.531	590.41	2.972	629.90	5.206	605.80	6.393
398.31	0.997	400.41	1.039	426.44	1.736	622.67	3.206	666.41	5.697	637.77	6.992
401.94	1.079	406.34	1.167	433.54	1.972	645.56	3.365	679.56	5.888	676.99	7.724
407.15	1.138	412.35	1.315	438.36	2.157						
ρ/kg·m^{-3} = 158.30		ρ/kg·m^{-3} = 189.90		ρ/kg·m^{-3} = 253.20		ρ/kg·m^{-3} = 158.30		ρ/kg·m^{-3} = 189.90		ρ/kg·m^{-3} = 253.20	
317.26	0.0605	310.18	0.060	307.45	0.040	415.62	1.559	467.51	3.681	468.13	4.039
340.65	0.236	337.32	0.201	337.25	0.230	420.15	1.708	468.56	3.765	473.05	4.334
346.52	0.280	351.23	0.337	361.68	0.520	433.54	2.131	473.56	4.069	484.84	5.118
355.48	0.374	362.53	0.460	375.93	0.767	445.11	2.557	484.27	4.598	506.82	6.579
360.77	0.429	376.25	0.671	380.82	0.857	457.35	3.033	507.44	5.726	540.65	8.834
364.29	0.463	388.95	0.878	389.70	1.016	463.34	3.248	544.15	7.000	574.15	10.893
368.45	0.508	394.77	1.000	390.79	1.049	466.16	3.375	572.09	8.216	607.12	12.697
371.71	0.554	401.85	1.147	391.87	1.103	475.84	3.740	607.79	9.492	645.60	14.913
376.03	0.613	407.31	1.328	394.90	1.177	486.49	4.129	644.95	10.874	678.67	16.047
379.38	0.660	412.27	1.445	400.65	1.315	492.51	4.336	674.78	12.052		
383.09	0.736	413.71	1.483	407.39	1.531	497.61	4.507				
387.50	0.827	414.79	1.539	420.40	1.933	516.97	5.138				
390.59	0.905	420.55	1.795	432.74	2.403	539.61	5.815				
394.20	0.991	431.62	2.295	444.09	2.834	570.01	6.641				
395.58	1.018	444.00	2.854	449.92	3.083	605.80	7.660				
399.83	1.134	455.96	3.323	456.51	3.374	640.44	8.600				
407.20	1.322	462.29	3.500	460.46	3.538	677.19	9.651				
410.90	1.429	466.19	3.633	461.65	3.614						
ρ/kg·m^{-3} = 316.50		ρ/kg·m^{-3} = 379.80		ρ/kg·m^{-3} = 443.00		ρ/kg·m^{-3} = 316.50		ρ/kg·m^{-3} = 379.80		ρ/kg·m^{-3} = 443.00	
309.26	0.048	305.85	0.0393	310.10	0.0485	437.75	2.608	426.35	2.216	440.16	3.393
338.82	0.254	306.98	0.0432	336.66	0.234	443.79	2.844	431.88	2.472	453.41	5.579
363.25	0.500	335.78	0.232	349.69	0.373	447.83	3.087	432.60	2.482	476.27	10.000
366.90	0.552	349.29	0.358	356.16	0.439	449.97	3.226	444.01	3.059	499.36	14.736
370.38	0.610	358.39	0.466	360.35	0.510	455.96	3.559	455.55	3.775	522.99	20.205
374.83	0.700	364.06	0.546	364.23	0.562	460.81	3.825	467.44	5.039	543.19	24.657
375.61	0.739	367.76	0.615	367.75	0.614	473.02	4.697	490.82	8.295	576.59	31.618
382.14	0.855	371.49	0.688	372.31	0.707	486.01	5.677	525.06	12.913	604.86	40.508
388.25	1.000	375.56	0.757	378.30	0.825	505.65	7.590	525.40	13.079	637.57	49.164
394.52	1.068	382.35	0.902	390.40	1.095	528.39	9.834	558.84	17.657	677.68	60.000
400.37	1.300	395.79	1.197	398.43	1.298	562.86	13.138	593.55	22.500		
408.27	1.516	407.91	1.539	399.82	1.340	596.42	15.933	625.40	26.559		
414.16	1.716	415.18	1.802	403.92	1.492	629.73	18.893	645.84	29.393		
420.40	1.893	416.49	1.851	414.64	1.893	664.86	21.978	673.86	33.089		
425.52	2.118	418.96	1.952	427.72	2.492	678.17	23.159				
431.05	2.325	419.96	2.039	427.82	2.492						
$x = 0.8570$ mole fraction of n-C_5H_{12}											
ρ/kg·m^{-3} = 63.55						ρ/kg·m^{-3} = 63.55					
310.96	0.058					425.77	1.638				
336.16	0.204					431.64	1.736				
349.89	0.355					438.03	1.815				
356.59	0.442					443.99	1.933				
363.15	0.511					455.40	2.088				
370.26	0.598					479.90	2.413				
375.82	0.645					512.90	2.913				
382.83	0.738					548.15	3.393				
388.58	0.883					581.46	3.745				
400.50	1.098					602.89	3.952				
414.81	1.393					646.54	4.256				
419.51	1.492					678.27	4.442				
$x = 0.139$ mole fraction of n-C_5H_{12}											
ρ/kg·m^{-3} = 78.24		ρ/kg·m^{-3} = 117.36		ρ/kg·m^{-3} = 162.06		ρ/kg·m^{-3} = 78.24		ρ/kg·m^{-3} = 117.36		ρ/kg·m^{-3} = 162.06	
314.12	0.044	310.61	0.041	311.79	0.043	464.97	2.579	523.44	6.354	443.19	2.775
345.41	0.279	336.71	0.205	337.67	0.215	476.63	2.972	547.97	8.492	470.35	3.834
363.50	0.525	362.29	0.508	362.65	0.520	488.36	3.472	558.00	9.638	473.95	5.078
376.86	0.758	391.71	1.052	390.75	1.008	500.31	4.059	562.59	10.059	517.92	6.601
382.35	0.855	402.90	1.285	397.82	1.157	511.15	4.697	564.92	10.354	540.59	8.500
386.55	0.929	406.65	1.374	402.96	1.295	523.15	5.433	568.44	10.697	565.53	11.216
390.66	1.020	409.86	1.413	405.82	1.354	534.12	6.197	572.26	11.236	577.43	12.393
397.06	1.138	410.71	1.433	410.52	1.511	544.57	7.000	576.56	11.539	580.79	12.834
401.26	1.236	415.71	1.588	413.43	1.588	568.75	8.374	579.51	11.775	587.70	13.893
403.76	1.298	420.55	1.726	444.95	1.647	573.36	9.000	592.15	13.138	589.51	14.187
406.87	1.328	420.36	1.884	448.35	1.803	576.75	9.078	610.10	14.579	592.30	14.550
416.93	1.442	430.10	2.039	423.60	2.010	591.21	9.657	634.97	16.236	598.16	15.275
427.59	1.598	436.57	2.236	424.84	2.108	613.84	10.500	659.16	17.834	624.77	18.315
427.86	1.638	455.34	2.795	430.06	2.315	636.61	11.393	677.93	19.078	674.15	24.059
441.47	1.933	483.89	3.756	433.54	2.433	675.82	12.908				
451.00	2.177	500.95	4.795	441.96	2.641						

Table 2. Continued

T/K	*P*/MPa	*T*/K	*P*/MPa	*T*/K	*P*/MPa	*T*/K	*P*/MPa	*T*/K	*P*/MPa	*T*/K	*P*/MPa
ρ/kg·m^{-3} = 202.57		ρ/kg·m^{-3} = 243.09		ρ/kg·m^{-3} = 324.12		ρ/kg·m^{-3} = 202.57		ρ/kg·m^{-3} = 243.09		ρ/kg·m^{-3} = 324.12	
310.65	0.043	310.49	0.043	310.63	0.043	563.99	11.795	510.21	7.236	505.64	7.638
337.90	0.240	340.69	0.240	340.36	0.238	570.65	12.657	536.41	9.492	529.99	10.059
363.49	0.537	366.44	0.571	366.62	0.571	576.77	13.452	547.98	10.677	540.89	11.295
392.61	1.059	392.30	1.059	393.79	1.078	587.38	14.874	554.72	11.500	553.17	13.000
418.69	1.815	418.12	1.775	410.15	1.500	593.16	15.672	559.66	12.078	558.72	13.697
421.82	1.946	424.29	2.059	416.52	1.716	595.82	16.068	562.95	12.598	564.65	14.559
424.86	2.071	430.15	2.334	423.20	1.972	598.57	16.457	566.52	13.118	568.52	15.078
426.22	2.138	433.19	2.472	433.94	2.500	611.26	18.079	568.05	13.236	574.75	16.078
432.55	2.393	437.32	2.697	440.66	2.854	624.71	19.795	576.74	14.559	587.29	17.893
438.35	2.695	441.00	2.854	446.99	3.256	650.49	22.928	589.38	16.492	609.25	22.334
451.17	3.315	444.50	3.078	450.84	3.433	674.72	26.031	604.31	19.031	615.03	23.802
475.62	4.472	451.05	3.452	455.40	3.736			607.37	19.453	618.16	24.394
499.27	5.893	453.74	3.581	458.55	4.039			617.62	20.893	628.44	26.367
520.57	7.598	456.49	3.715	462.29	4.315			640.15	24.157	647.65	30.236
544.52	9.697	462.45	4.118	467.76	4.775			677.40	29.426	673.87	35.653
558.42	11.098	486.90	5.472	480.50	5.578						
ρ/kg·m^{-3} = 405.15		ρ/kg·m^{-3} = 486.17		ρ/kg·m^{-3} = 567.20		ρ/kg·m^{-3} = 405.15		ρ/kg·m^{-3} = 486.17		ρ/kg·m^{-3} = 567.20	
308.74	0.038	309.86	0.039	308.27	0.0375	538.02	12.393	543.71	15.893	515.15	16.039
340.49	0.241	338.80	0.221	339.74	0.239	549.70	14.177	547.34	17.177	526.94	19.197
364.26	0.538	362.11	0.509	362.50	0.513	553.99	14.992	549.65	17.472	533.04	20.933
392.01	1.045	392.51	1.053	400.89	1.240	556.45	15.559	554.79	18.697	536.57	22.374
423.05	2.000	427.30	2.197	431.84	2.354	560.13	16.098	560.05	20.078	540.11	23.393
435.36	2.539	440.29	2.893	444.36	3.138	567.45	17.393	571.84	23.098	544.40	24.657
448.07	3.236	444.55	3.138	448.62	3.395	577.36	19.539	583.51	26.500	547.70	25.657
455.43	3.697	451.29	3.559	452.31	3.531	602.00	25.039	595.35	30.079	555.34	28.393
460.42	4.098	458.50	3.933	454.50	3.664	613.16	28.039	606.85	34.500	557.40	29.677
464.50	4.539	464.65	4.433	457.07	4.078	626.16	31.933	630.24	43.775	561.82	30.786
467.37	4.756	470.40	4.952	457.37	4.131	629.49	32.933	632.36	45.608	566.07	33.157
469.62	4.952	475.92	5.756	460.17	4.677	640.41	36.452	636.39	47.147	579.76	38.874
477.36	5.472	482.53	6.393	467.57	5.697	647.66	38.834	647.49	51.577	591.17	43.598
488.65	6.578	493.41	7.933	478.90	7.795	675.19	47.618	669.39	60.518	614.06	51.674
513.49	9.354	519.50	11.472	503.07	13.059					634.88	60.478
ρ/kg·m^{-3} = 607.70		ρ/kg·m^{-3} = 648.23				ρ/kg·m^{-3} = 607.70		ρ/kg·m^{-3} = 648.23			
308.48	0.0377	309.49	0.038			483.11	11.736	451.50	7.972		
338.39	0.217	338.00	0.215			508.37	19.736	463.67	12.452		
363.37	0.525	362.92	0.518			533.79	28.638	477.10	17.393		
392.14	1.049	382.60	1.078			538.31	30.492	489.25	22.000		
423.19	2.017	407.25	1.374			541.84	32.000	501.46	26.677		
435.95	2.618	419.14	1.834			546.15	33.697	513.04	39.177		
442.67	2.972	423.49	2.018			549.52	35.098	524.55	38.834		
446.12	3.236	427.82	2.198			553.16	36.559	536.35	44.697		
450.49	3.795	429.15	2.256			556.67	38.197	548.59	50.000		
453.92	4.539	430.17	2.477			562.98	41.039	544.71	48.177		
460.56	5.992	432.01	2.834			574.77	47.413	553.41	52.393		
461.32	8.697	438.91	4.500			582.79	51.972	556.90	54.598		
				x = 0.1185 mole fraction of n-C_5H_{12}							
ρ/kg·m^{-3} = 82.60		ρ/kg·m^{-3} = 123.94		ρ/kg·m^{-3} = 165.20		ρ/kg·m^{-3} = 82.60		ρ/kg·m^{-3} = 123.94		ρ/kg·m^{-3} = 165.20	
312.41	0.045	311.95	0.044	310.66	0.042	564.49	8.791	564.52	9.756	412.46	1.618
338.51	0.218	339.16	0.225	339.13	0.242	565.17	8.875	567.95	10.177	414.77	1.736
366.41	0.505	350.61	0.343	363.95	0.500	572.98	9.374	572.73	10.697	424.36	2.059
379.43	0.765	367.62	0.520	365.66	0.510	578.49	9.736	576.23	10.933	451.85	3.000
383.55	0.900	378.16	0.743	368.79	0.608	591.74	10.618	580.36	11.334	476.61	3.952
385.29	0.967	383.55	0.842	377.59	0.745	612.86	11.638	585.65	12.059	500.90	5.138
386.34	1.020	387.59	1.177	383.05	0.852	637.86	12.638	596.70	13.354	522.75	6.697
387.82	1.044	391.32	1.275	383.76	0.864	658.21	13.502	619.90	15.472	546.96	8.815
390.35	1.078	396.59	1.374	387.86	0.965	675.15	14.223	643.97	17.236	570.59	11.315
392.13	1.118	403.10	1.539	388.93	0.981			662.00	18.502	576.43	12.000
396.46	1.206	416.62	1.893	394.85	1.157			677.73	19.617	580.21	12.393
401.86	1.295	428.73	2.256	395.09	1.197					584.55	12.893
415.12	1.500	438.22	2.520	396.47	1.216					587.75	13.295
440.67	1.952	463.71	3.157	399.51	1.256					591.61	13.795
464.32	2.539	486.48	4.098	401.52	1.285					597.21	14.539
489.97	3.452	511.48	5.334	404.19	1.354					607.37	15.874
513.96	4.657	534.47	7.078	405.68	1.384					618.96	17.177
538.44	6.256	558.55	9.177	408.99	1.492					647.83	19.834
561.17	8.354	560.65	9.492	409.58	1.520					674.79	21.935
ρ/kg·m^{-3} = 206.60		ρ/kg·m^{-3} = 247.90		ρ/kg·m^{-3} = 330.50		ρ/kg·m^{-3} = 206.60		ρ/kg·m^{-3} = 247.90		ρ/kg·m^{-3} = 330.50	
310.56	0.042	310.59	0.042	310.13	0.041	514.05	6.559	460.67	4.000	618.00	23.657
339.8	0.255	339.22	0.238	340.22	0.251	537.91	8.472	463.67	4.039	624.09	25.138
369.45	0.539	364.51	0.547	367.81	0.569	562.26	10.736	469.72	4.354	629.94	26.433
379.41	0.772	381.29	0.798	393.63	1.059	572.43	11.972	483.19	5.118	635.15	27.636
386.87	0.919	393.19	1.059	420.41	1.933	579.45	13.02	507.30	6.716	645.95	30.500
393.39	1.078	406.91	1.482	433.65	2.492	583.12	13.677	530.26	8.500	657.17	33.295
399.89	1.236	411.86	1.657	446.02	3.098	587.18	14.098	566.71	12.618	675.82	38.114
404.6	1.344	414.90	1.805	453.15	3.539	590.85	14.697	578.86	14.197		
407.16	1.452	418.75	1.923	458.17	3.933	594.77	15.197	584.21	15.177		
412.2	1.618	422.81	2.078	461.40	4.138	598.32	15.893	589.82	16.039		
415.9	1.736	426.71	2.216	465.33	4.413	605.13	17.098	595.73	16.992		
420.09	1.874	430.70	2.393	468.95	4.697	607.28	17.551	601.61	17.933		
423.66	2.098	434.72	2.578	475.69	5.098	611.42	18.222	607.59	18.992		
430.15	2.354	738.52	2.775	485.98	5.775	617.31	19.197	613.45	20.334		
441.71	2.874	442.29	2.933	510.14	7.736	620.15	19.561	619.21	21.433		
444.86	3.033	445.99	3.138	535.50	10.098	640.07	22.011	625.12	22.500		
450.17	3.235	449.79	3.374	558.40	13.078	655.25	23.993	631.04	23.393		
466.42	3.834	453.35	3.618	583.50	16.638	675.72	25.588	642.05	25.197		
490.35	4.992	457.00	3.854	606.34	20.834			675.00	29.815		

Table 2. Continued

T/K	*P*/MPa	*T*/K	*P*/MPa	*T*/K	*P*/MPa	*T*/K	*P*/MPa	*T*/K	*P*/MPa	*T*/K	*P*/MPa
ρ/kg·m^{-3} = 413.10		ρ/kg·m^{-3} = 496.00		ρ/kg·m^{-3} = 578.00		ρ/kg·m^{-3} = 413.10		ρ/kg·m^{-3} = 496.00		ρ/kg·m^{-3} = 578.00	
309.69	0.039	309.70	0.039	309.30	0.0387	534.65	11.578	487.15	6.845	521.50	16.893
340.13	0.260	340.17	0.265	338.82	0.245	559.68	15.315	512.07	10.618	546.42	23.893
366.06	0.568	368.09	0.573	367.12	0.571	582.49	19.697	537.29	14.736	569.71	32.795
393.32	1.059	395.06	1.069	392.96	1.039	605.32	25.000	561.70	19.539	573.17	44.197
419.50	1.893	420.19	1.933	420.16	1.874	618.06	28.539	586.72	26.256	600.29	47.295
433.85	2.472	425.73	2.118	443.86	3.059	624.40	30.492	608.40	34.952	603.75	49.236
445.84	3.098	435.70	2.697	450.41	3.433	630.18	32.539	618.30	39.177	607.56	51.501
456.95	3.815	449.90	3.393	456.61	3.795	633.60	34.039	626.15	42.500	610.96	53.118
462.00	4.275	454.91	3.815	460.41	4.295	636.05	35.059	629.85	43.795	613.51	55.197
464.49	4.472	457.05	4.020	464.42	4.638	639.77	36.354	633.28	45.295	616.99	57.472
467.37	4.677	461.41	4.362	467.98	5.118	643.59	37.657	637.18	47.000	620.80	60.254
473.12	5.138	464.77	4.677	474.09	5.992	655.71	41.413	642.90	49.578		
484.29	6.098	469.71	5.020	487.02	7.992	674.00	47.215	654.47	55.500		
510.17	8.520	475.91	5.756	497.65	10.295			663.77	60.357		
ρ/kg·m^{-3} = 611.40		ρ/kg·m^{-3} = 661.00				ρ/kg·m^{-3} = 611.40		ρ/kg·m^{-3} = 661.00			
309.63	0.0388	309.71	0.039			448.09	3.197	443.22	4.736		
340.03	0.257	339.92	0.251			451.61	3.354	470.02	12.874		
366.75	0.550	366.84	0.551			455.59	3.854				
392.17	1.029	391.83	1.025			459.27	4.559				
419.36	1.874	418.15	1.824			462.90	5.138				
433.00	2.315	426.79	2.197			467.76	6.059				
436.40	2.578	430.05	2.374			473.59	7.216				
440.22	2.854	433.62	2.597			485.65	10.059				
444.25	3.078	437.86	3.578								
x = 0.0967 mole fraction of n-C_5H_{12}											
ρ/kg·m^{-3} = 84.77		ρ/kg·m^{-3} = 127.00		ρ/kg·m^{-3} = 169.30		ρ/kg·m^{-3} = 84.77		ρ/kg·m^{-3} = 127.00		ρ/kg·m^{-3} = 169.30	
305.25	0.037	309.59	0.040	309.72	0.040	579.96	8.364	480.77	3.433	465.76	3.511
335.06	0.203	340.03	0.245	337.86	0.215	590.71	9.000	502.93	4.539	478.28	4.127
360.16	0.442	366.47	0.548	365.12	0.517	615.99	10.657	525.93	6.078	503.16	5.472
365.75	0.520	373.32	0.657	392.22	1.037	638.32	12.138	550.41	7.993	527.40	7.031
373.02	0.651	376.02	0.696	396.66	1.157	661.19	13.618	563.84	9.216	548.90	9.137
379.67	0.687	379.14	0.741	403.36	1.315	676.82	14.638	567.05	9.598	562.39	10.393
382.22	0.715	381.84	0.799	408.10	1.452			570.05	9.952	575.85	11.559
389.69	0.831	384.42	0.831	411.14	1.559			571.29	10.078	578.01	11.932
401.81	1.030	386.71	0.883	412.70	1.610			575.77	10.561	580.77	12.334
427.15	1.433	389.66	0.940	416.45	1.757			575.71	10.559	583.16	12.696
452.35	1.893	392.65	1.000	418.17	1.795			577.63	11.020	585.82	13.137
478.06	2.539	394.65	1.051	421.32	1.952			582.04	11.197	586.92	13.255
501.66	3.578	397.89	1.138	422.71	2.000			583.39	11.315	595.43	14.334
525.51	5.020	400.05	1.197	425.25	2.118			586.80	11.657	621.67	17.991
549.42	6.529	402.67	1.275	428.32	2.295			589.21	12.039	642.57	20.952
555.19	6.952	405.19	1.315	430.27	2.314			597.97	13.236		
561.05	7.303	408.08	1.393	432.85	2.371			608.73	14.492		
563.55	7.472	411.61	1.500	436.42	2.452			631.56	16.677		
567.43	7.677	416.98	1.638	438.65	2.539			643.39	17.677		
570.35	7.834	429.74	1.933	441.80	2.657			661.40	19.051		
573.86	7.992	455.20	2.520	454.62	3.039			677.26	20.234		
ρ/kg·m^{-3} = 211.62		ρ/kg·m^{-3} = 253.94		ρ/kg·m^{-3} = 338.59		ρ/kg·m^{-3} = 211.62		ρ/kg·m^{-3} = 253.94		ρ/kg·m^{-3} = 338.59	
309.71	0.040	309.41	0.040	309.25	0.040	563.97	11.295	547.24	9.952	547.63	11.500
338.05	0.221	338.04	0.223	338.01	0.222	570.59	12.039	548.59	10.157	550.84	11.834
366.41	0.518	365.63	0.519	365.69	0.523	573.52	12.432	552.15	10.559	553.36	12.196
392.31	1.059	390.89	1.029	391.98	1.029	575.15	12.598	556.19	10.972	557.34	12.736
417.76	1.795	417.79	1.795	417.92	1.756	576.30	12.716	557.70	11.157	566.79	14.196
443.71	2.814	444.61	2.933	444.50	2.933	577.99	12.991	560.61	11.491	590.74	18.098
446.39	2.972	446.02	3.039	449.47	3.295	582.67	13.491	563.13	11.834	591.55	18.314
447.61	3.019	448.95	3.256	452.14	3.472	586.82	14.216	565.86	12.255	604.95	20.736
450.44	3.138	451.26	3.413	454.49	3.650	600.48	16.196	568.15	12.452	618.41	23.578
453.12	3.314	453.45	3.539	456.97	3.814	620.69	19.598	568.56	12.393	622.36	24.295
454.91	3.393	456.18	3.677	459.50	4.020	648.41	23.991	568.95	12.432	626.67	25.393
458.11	3.472	458.46	3.795	462.35	4.196	674.88	28.236	569.24	12.452	629.28	26.031
460.97	3.578	460.95	3.854	464.90	4.334			572.69	12.932	631.09	26.118
463.09	3.677	463.36	4.000	467.38	4.472			574.16	13.237	634.16	27.598
469.13	3.893	467.71	4.177	469.55	4.618			580.54	14.000	642.94	29.696
480.72	4.519	470.77	4.354	475.61	4.972			592.21	15.696	654.82	32.452
505.21	5.893	486.52	5.177	487.56	5.795			618.05	20.716	674.73	37.236
528.66	7.598	502.53	6.196	510.20	7.618			648.08	26.314		
552.78	9.913	531.50	8.432	534.61	10.059			675.02	31.295		
ρ/kg·m^{-3} = 423.24		ρ/kg·m^{-3} = 507.88		ρ/kg·m^{-3} = 592.53		ρ/kg·m^{-3} = 423.24		ρ/kg·m^{-3} = 507.88		ρ/kg·m^{-3} = 592.53	
309.30	0.040	308.26	0.040	305.37	0.037	556.17	14.413	552.47	16.834	468.99	5.177
337.87	0.220	337.92	0.221	337.99	0.222	578.77	18.354	578.95	23.137	482.07	7.472
363.29	0.511	365.66	0.520	365.26	0.517	579.94	18.578	605.27	31.559	505.84	11.696
392.04	1.039	392.11	1.029	392.13	1.039	581.02	18.696	614.59	35.893	529.44	17.531
418.15	1.795	417.72	1.814	417.40	1.795	602.00	23.432	616.93	37.000	552.84	25.236
443.42	3.000	443.32	2.991	431.19	2.373	613.00	26.098	626.50	41.137	577.90	36.295
449.36	3.334	445.91	3.157	438.49	2.637	623.45	28.873	633.66	43.196	590.42	43.295
451.67	3.500	449.15	3.393	439.41	2.795	623.67	29.000	649.97	48.000	600.96	51.000
454.46	3.657	451.17	3.491	443.26	3.000	625.35	29.500	659.18	50.598	606.90	54.500
456.88	3.834	453.80	3.637	444.82	3.098	628.37	30.637	664.26	52.118	615.66	60.000
459.52	4.078	456.07	3.814	448.89	3.393	632.15	31.578				
461.91	4.275	458.90	4.078	450.15	3.432	635.41	32.500				
465.11	4.432	461.55	4.314	452.69	3.618	636.43	32.795				
467.52	4.598	464.03	4.472	456.01	3.814	638.83	33.598				
473.30	5.039	468.99	4.854	457.50	3.932	643.65	34.932				
485.51	6.137	481.49	6.098	459.65	4.118	656.82	38.693				
508.71	8.472	506.77	9.295	460.71	4.186	673.80	43.618				
532.65	11.354	527.80	12.500	462.45	4.472						

Table 2. Continued

T/K	*P*/MPa	*T*/K	*P*/MPa	*T*/K	*P*/MPa	*T*/K	*P*/MPa	*T*/K	*P*/MPa	*T*/K	*P*/MPa
ρ/kg·m^{-3} = 550.20		ρ/kg·m^{-3} = 677.18				ρ/kg·m^{-3} = 550.20		ρ/kg·m^{-3} = 677.18			
307.55	0.039	308.68	0.040			512.35	11.736				
337.99	0.221	337.85	0.219			534.45	16.696				
365.55	0.519	363.77	0.496			558.55	22.491				
392.20	1.039	389.35	1.000			581.93	30.393				
415.25	1.706	414.86	1.795			606.40	40.775				
439.58	2.814	433.31	2.696			619.04	47.039				
446.00	3.177	437.32	3.196			623.39	48.991				
448.36	3.334	441.52	3.854			626.17	49.334				
450.85	3.578	444.56	5.295			628.82	52.255				
453.15	3.775	450.16	7.196			631.39	53.245				
455.32	3.913					632.52	54.509				
457.55	4.039					634.56	55.177				
460.22	4.334					636.69	55.618				
466.22	4.893					642.87	57.893				
488.62	7.834					649.18	60.019				
x = 0.075 mole fraction of n-C_5H_{12}											
ρ/kg·m^{-3} = 87.14		ρ/kg·m^{-3} = 174.28		ρ/kg·m^{-3} = 217.80		ρ/kg·m^{-3} = 87.14		ρ/kg·m^{-3} = 174.28		ρ/kg·m^{-3} = 217.80	
307.36	0.039	309.49	0.040	307.39	0.037	500.64	4.288	596.55	17.388	439.49	2.691
335.38	0.213	334.05	0.196	334.49	0.215	511.93	5.068	602.65	17.899	442.04	2.754
362.06	0.486	360.35	0.469	362.09	0.501	523.50	5.864	607.52	18.787	449.65	2.977
375.50	0.731	373.70	0.695	375.02	0.726	535.21	6.815	613.31	19.992	470.31	3.788
377.49	0.779	381.05	0.835	387.36	0.995	545.97	7.874	618.05	20.559	493.25	5.104
378.75	0.781	387.36	0.980	388.03	1.001	557.84	9.136	626.89	21.433	528.14	7.891
380.29	0.785	388.79	1.021	391.55	1.098	568.95	10.401	636.46	22.638	562.26	11.471
383.18	0.802	392.55	1.111	393.46	1.147	580.95	11.846	648.91	24.039	584.81	14.947
386.15	0.835	395.76	1.183	399.36	1.295	592.42	13.300	674.73	26.849	596.19	17.054
388.18	0.862	400.66	1.289	406.19	1.472	594.91	13.693			607.72	19.312
393.66	0.921	405.95	1.478	412.65	1.677	597.43	13.775			613.92	20.587
406.06	1.309	419.77	1.893	416.06	1.795	603.26	14.098			619.81	21.793
417.84	1.411	442.94	2.501	418.45	1.859	613.82	14.736			622.20	22.189
430.65	1.723	466.29	3.321	418.86	1.874	635.42	16.039			625.54	22.748
442.66	1.905	488.92	4.736	422.41	2.021	668.34	17.893			631.10	23.874
454.19	2.273	522.19	7.512	425.21	2.108					640.98	25.002
465.88	2.674	555.87	10.902	429.40	2.275					651.30	27.216
478.22	3.165	578.52	13.898	436.27	2.579					676.17	31.538
488.94	3.692	590.80	15.871	437.21	2.657						
ρ/kg·m^{-3} = 261.40		ρ/kg·m^{-3} = 348.50		ρ/kg·m^{-3} = 435.70		ρ/kg·m^{-3} = 261.40		ρ/kg·m^{-3} = 348.50		ρ/kg·m^{-3} = 435.70	
307.61	0.037	307.5	0.037	303.46	0.035	541.61	9.287	543.26	10.401	619.93	27.861
334.63	0.215	335.26	0.216	337.56	0.231	569.19	12.603	577.86	15.022	622.67	28.783
360.56	0.497	360.72	0.492	362.51	0.504	576.65	13.698	612.81	22.273	625.95	29.697
387.86	0.962	388.18	0.984	387.14	0.981	590.59	15.985	618.54	23.752	629.47	30.433
412.66	1.675	413.86	1.697	412.54	1.661	598.91	17.566	624.25	25.247	633.06	31.138
438.65	2.665	438.16	2.657	437.86	2.664	604.40	18.712	630.61	26.805	638.59	33.157
450.55	3.381	457.42	3.738	450.34	3.281	610.54	19.976	635.97	27.716	650.18	36.854
451.57	3.391	458.77	3.881	456.83	3.705	621.48	22.405	641.75	29.216	661.82	40.697
453.19	3.424	458.81	3.883	462.97	4.241	625.27	23.316	647.35	30.598	675.50	45.049
456.26	3.511	461.82	4.051	465.17	4.354	627.17	23.735	664.45	35.157		
461.71	3.671	462.65	4.082	467.48	4.527	633.04	25.098				
467.94	3.986	464.26	4.141	473.36	5.025	634.50	25.354				
473.96	4.275	465.91	4.212	485.34	5.842	638.65	26.098				
484.72	4.752	467.73	4.288	509.08	7.752	641.60	26.736				
507.07	6.177	472.77	4.631	543.21	11.756	650.15	28.236				
508.26	6.201	483.81	5.413	578.07	17.703	670.82	31.393				
529.90	8.103	508.12	6.893	613.95	26.381	684.20	34.204				
ρ/kg·m^{-3} = 522.90		ρ/kg·m^{-3} = 609.97		ρ/kg·m^{-3} = 188.05		ρ/kg·m^{-3} = 522.90		ρ/kg·m^{-3} = 609.97		ρ/kg·m^{-3} = 188.05	
309.78	0.041	314.32	0.044	310.61	0.041	547.95	14.686	507.45	9.806	458.35	4.334
336.49	0.245	334.15	0.232	336.63	0.247	583.15	22.391	543.15	17.644	462.05	5.177
362.93	0.497	362.99	0.483	362.36	0.479	605.73	29.276	578.62	28.736	474.25	7.765
389.42	1.035	389.20	1.031	388.46	1.016	612.15	31.802	601.83	29.057	497.40	14.338
414.20	1.701	414.11	1.697	415.31	1.755	614.57	32.833	623.15	52.786	520.84	22.913
438.27	2.663	439.41	2.721	427.65	2.198	620.27	35.001	625.86	54.436	542.75	33.286
462.77	4.305	451.52	3.377	434.11	2.481	631.49	40.315	628.09	56.477	579.30	54.939
465.14	4.374	458.39	3.834	439.88	2.756	654.70	50.452	629.65	57.001	592.82	62.866
467.79	4.521	461.09	4.059	446.15	3.098	675.51	59.923	632.37	59.338		
471.27	4.834	464.09	4.481	452.32	3.387			634.58	61.324		
478.14	5.526	466.46	4.657	452.50	3.393			634.66	61.333		
489.00	6.585	472.64	5.138	454.85	3.736			636.94	63.039		
511.90	9.101	483.61	6.425	455.70	3.933						
x = 0.058 mole fraction of n-C_5H_{12}											
ρ/kg·m^{-3} = 89.21		ρ/kg·m^{-3} = 178.42		ρ/kg·m^{-3} = 267.21		ρ/kg·m^{-3} = 89.21		ρ/kg·m^{-3} = 178.42		ρ/kg·m^{-3} = 267.21	
309.79	0.049	310.86	0.051	310.21	0.050	561.91	8.255	546.40	8.147	466.15	3.775
340.63	0.251	341.85	0.259	345.65	0.331	564.48	8.795	556.59	9.137	487.97	4.834
351.48	0.362	364.79	0.514	366.21	0.565	567.80	8.581	563.45	9.795	512.64	6.433
358.35	0.431	370.92	0.601	393.05	1.078	569.49	8.669	569.25	10.472	535.78	8.137
364.89	0.511	376.21	0.691	397.78	1.186	571.65	8.795	570.59	10.598	558.45	10.393
370.86	0.577	381.42	0.785	400.87	1.275	574.73	9.019	575.10	11.098	589.45	14.334
374.72	0.631	385.15	0.863	404.56	1.413	577.49	9.314	582.79	12.049	593.96	15.078
379.11	0.671	389.39	0.962	405.51	1.452	583.96	9.932	584.71	12.255	598.76	15.795
383.87	0.706	393.86	1.079	412.37	1.657	594.55	10.952	587.95	12.795	603.10	16.578
388.15	0.749	397.39	1.167	415.31	1.755	613.57	12.432	592.07	13.354	606.95	17.393
394.44	0.801	399.88	1.255	420.79	1.972	645.13	14.432	596.15	14.059	613.40	18.354
407.58	0.938	405.72	1.452	426.05	2.157	645.27	14.472	599.75	14.374	617.28	19.078
433.42	1.256	412.01	1.598	429.55	2.314	674.83	15.874	602.75	14.893	620.90	19.874
457.71	2.667	422.41	1.844	433.05	2.452			607.59	15.893	625.45	20.795
482.46	3.795	446.86	2.452	437.07	2.637			623.30	18.696	628.92	21.492
506.79	5.295	473.40	3.256	440.96	2.834			652.55	22.874	632.68	22.275
530.90	7.059	496.00	4.374	444.72	2.972			675.72	26.129	649.95	26.098
552.59	7.696	519.92	5.913	447.85	3.078					674.50	31.326
558.65	7.991	544.16	7.932	454.71	3.334						

Table 2. Continued

T/K	*P*/MPa	*T*/K	*P*/MPa	*T*/K	*P*/MPa	*T*/K	*P*/MPa	*T*/K	*P*/MPa	*T*/K	*P*/MPa
ρ/kg·m^{-3} = 356.80		ρ/kg·m^{-3} = 446.05		ρ/kg·m^{-3} = 535.26		ρ/kg·m^{-3} = 356.80		ρ/kg·m^{-3} = 446.05		ρ/kg·m^{-3} = 535.26	
310.66	0.051	310.63	0.051	310.56	0.050	573.08	13.598	615.51	24.818	586.55	24.255
339.11	0.252	339.15	0.252	339.08	0.252	596.31	17.539	628.99	28.736	595.27	26.677
365.81	0.565	367.02	0.571	366.62	0.571	601.37	18.501	634.10	30.539	602.02	29.098
391.62	1.059	393.83	1.078	392.97	1.059	611.81	20.393	638.68	32.059	604.66	30.000
417.67	1.854	421.42	1.932	417.67	1.854	614.79	21.078	642.10	33.393	611.73	32.736
431.06	2.393	434.42	2.442	426.27	2.157	624.12	23.177	644.19	34.098	614.86	34.098
439.11	2.775	439.10	2.736	452.21	3.559	627.26	23.785	650.28	36.874	616.21	34.677
441.40	2.874	451.00	3.452	458.34	4.000	630.85	24.492	651.68	37.137	620.55	36.492
446.61	3.196	461.15	4.216	462.55	4.334	634.96	25.647	661.35	40.893	621.59	37.157
451.15	3.500	417.15	4.539	467.59	4.755	638.05	26.736	674.86	46.255	623.05	37.874
455.25	3.755	467.58	4.618	469.94	4.972	641.04	27.775			624.56	38.696
459.79	3.992	468.89	4.736	474.16	5.354	643.13	28.137			628.65	40.598
462.79	4.118	476.87	5.275	478.71	5.736	647.44	29.041			634.04	43.049
465.55	4.314	504.75	7.432	488.77	6.736	652.21	30.236			640.37	46.196
477.31	4.932	530.67	10.59	509.35	9.059	653.16	30.716			648.90	50.098
501.86	6.539	554.45	13.196	536.14	12.992	656.34	31.598			660.49	55.295
527.09	8.598	580.00	17.137	555.19	16.354	665.50	36.737			671.17	60.196
551.60	10.893	606.50	22.559	577.81	21.834	674.52	34.157				
ρ/kg·m^{-3} = 579.87		ρ/kg·m^{-3} = 624.45		ρ/kg·m^{-3} = 713.68		ρ/kg·m^{-3} = 579.87		ρ/kg·m^{-3} = 624.45			
310.55	0.050	310.59	0.050	403.89	1.354	474.79	5.834	578.92	34.893		
339.15	0.253	339.05	0.252	416.50	1.893	485.31	7.000	602.20	48.696		
366.59	0.571	366.65	0.570	427.42	2.334	510.02	10.432	610.83	55.157		
392.86	1.088	392.75	1.885	440.80	3.078	531.66	14.334	617.86	60.696		
414.95	1.814	416.79	1.893	441.93	3.177	555.65	20.000				
441.45	3.137	429.61	2.500	443.71	3.559	579.86	27.039				
451.35	3.854	442.59	3.196	446.29	4.098	602.97	36.598				
453.52	3.972	454.75	3.932	450.45	4.874	625.46	49.393				
454.57	4.059	457.55	4.196	454.87	5.598	626.69	49.874				
456.60	4.186	461.55	4.618	469.20	9.854	628.92	50.696				
458.59	4.275	465.61	5.039	491.62	18.637	631.81	52.834				
459.41	4.363	472.92	5.992	516.15	31.137	632.26	52.932				
461.34	4.413	485.15	7.696	540.94	45.314	634.16	53.775				
462.44	4.598	507.70	11.579	559.80	60.196	641.40	57.598				
463.87	4.893	533.44	17.637			646.56	60.236				
467.39	5.098	554.95	24.736								
				x = 0.027 mole fraction of n-C_5H_{12}							
ρ/kg·m^{-3} = 94.20		ρ/kg·m^{-3} = 188.40		ρ/kg·m^{-3} = 282.65		ρ/kg·m^{-3} = 94.20		ρ/kg·m^{-3} = 188.40		ρ/kg·m^{-3} = 282.65	
310.36	0.050	313.93	0.0628	310.28	0.050	559.50	7.393	565.86	8.795	528.95	6.472
340.31	0.251	336.59	0.220	341.29	0.256	563.08	7.736	588.65	11.775	554.24	8.511
349.29	0.308	351.76	0.336	360.56	0.455	566.65	8.334	597.86	13.098	577.93	11.295
354.15	0.326	356.15	0.372	366.16	0.542	573.92	8.972	603.17	13.893	599.21	14.452
355.19	0.339	357.31	0.384	373.01	0.655	583.09	10.147	611.96	15.295	610.82	16.578
358.43	0.360	363.46	0.455	381.57	0.808	585.46	10.472	615.92	16.049	617.04	17.736
361.32	0.365	365.41	0.494	384.14	0.855	591.61	11.255	618.57	16.549	624.40	19.255
363.35	0.372	371.58	0.588	393.04	1.059	599.49	12.324	620.21	16.991	629.48	20.295
369.35	0.386	373.55	0.612	396.86	1.147	605.19	13.147	623.56	17.559	632.59	21.000
381.56	0.414	377.15	0.636	403.55	1.314	608.31	13.334	625.75	18.098	636.85	21.736
408.40	0.612	383.15	0.708	407.05	1.422	611.53	13.432	628.56	18.814	638.84	22.196
431.36	0.896	396.59	0.855	412.80	1.519	614.31	13.578	632.85	19.539	641.15	22.716
458.61	1.472	421.42	1.137	416.36	1.588	618.56	13.893	637.07	20.373	646.82	25.854
484.03	2.255	447.59	1.578	421.33	1.716	628.15	14.637	644.49	21.598	656.65	26.098
507.24	3.374	470.32	2.255	433.14	1.991	634.33	14.932	650.09	22.491	673.86	29.696
531.74	4.893	495.52	3.314	459.45	2.736	646.45	15.578	660.15	24.000		
554.65	6.913	518.22	4.677	485.26	3.736	674.82	16.795	675.43	26.016		
556.09	7.039	542.51	6.578	507.49	4.893						
ρ/kg·m^{-3} = 376.87		ρ/kg·m^{-3} = 471.10				ρ/kg·m^{-3} = 376.87		ρ/kg·m^{-3} = 471.10			
313.50	0.0617	311.63	0.0581			574.69	11.893	602.86	18.157		
343.35	0.262	341.16	0.245			597.63	15.236	600.95	18.177		
368.16	0.560	367.92	0.541			618.65	19.393	609.40	19.834		
395.32	1.098	394.81	1.078			520.36	19.696	614.41	20.795		
404.08	1.295	419.99	1.834			622.84	20.196	617.10	21.539		
408.69	1.472	425.60	2.059			624.42	20.557	622.57	22.657		
414.37	1.637	434.16	2.432			630.69	21.854	623.95	22.972		
420.15	1.834	438.71	2.677			628.32	21.500	626.35	23.578		
424.59	2.019	446.35	3.039			631.29	21.952	628.06	24.098		
430.74	2.196	451.47	3.314			632.78	22.216	630.07	24.736		
435.41	2.373	457.46	3.637			535.34	22.736	633.93	26.098		
439.28	2.519	462.77	3.913			644.55	25.295	637.75	27.500		
450.55	2.972	474.64	4.472			651.20	27.216	642.65	29.098		
477.16	4.039	500.38	6.118			653.69	27.873	656.93	34.157		
502.33	5.432	521.85	7.814			657.56	28.972	674.71	40.657		
531.29	7.452	544.74	9.913			674.83	33.736	620.77	22.295		
553.71	9.472	567.95	12.893					621.59	22.539		

Tables 3 and 4. Heating the three-phase (LLG) water + *n*-pentane mixture can lead to three different sequences of phase transitions, depending on the fill coefficient (ratio of the volume of the mixture to the volume of the piezometer at ambient temperature) or the average fill density (ratio of the mass of mixture to the volume of the piezometer at ambient temperature) and the *n*-pentane concentration in the initial mixture. The "breakpoints" on $P-T$ isochors are the phase boundary data (at the intersection of the phase boundary curve) connected with liquid−liquid (LL), LG, or LLG phase transitions occurring in a binary water + *n*-pentane mixture heated in a closed volume. Two peaks or jumps in the isochoric heat capacity are also often found in the system water + *n*-alkanes mixtures at isochoric heating.[35−37] The following sequences of the phase transitions are possible in the water + *n*-pentane mixture when the system is heated isochorically:

1. At the highest average densities and high concentrations of *n*-pentane, the liquid phase expands on heating and fills the

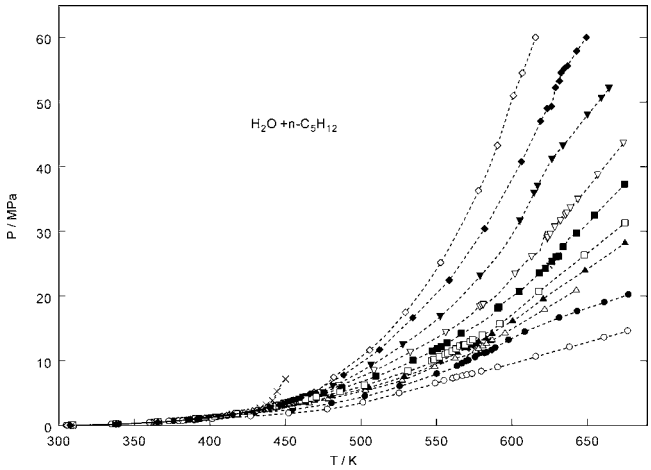

Figure 7. Measured pressures as a function of temperature along the various isochores for the selected concentration of 0.0967 mole fraction of n-C_5H_{12}. ●, 127.00 kg·m^{-3}; ○, 84.77 kg·m^{-3}; △, 169.30 kg·m^{-3}; ▲, 211.62 kg·m^{-3}; □, 253.94 kg·m^{-3}; ■, 338.59 kg·m^{-3}; ▼, 507.88 kg·m^{-3}; ▽, 423.24 kg·m^{-3}; ◆, 550.20 kg·m^{-3}; ◇, 592.53 kg·m^{-3}; ×, 677.18 kg·m^{-3}; ----, experimental curves.

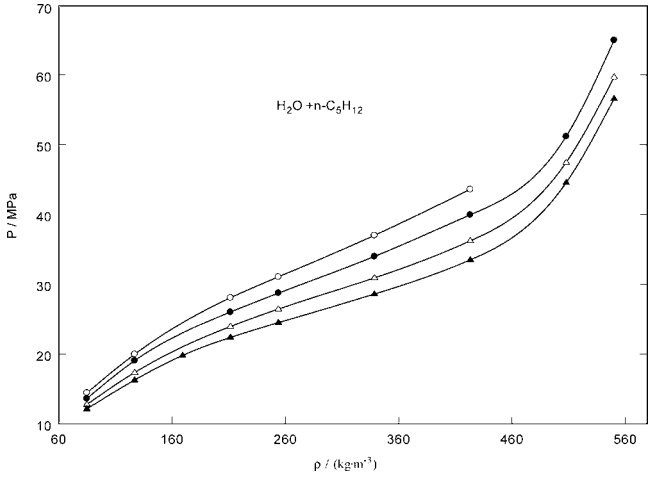

Figure 8. Measured pressures as a function of density along the supercritical isotherms for the selected concentration of 0.0967 mole fraction of n-C_5H_{12}. ●, 661.19 K; ○, 673.80 K; △, 648.18 K; ▲, 638.32 K; ----, smoothed experimental curves.

entire vessel, while the vapor phase disappears. A transition from three phases (LLG) to two phases (LL), (LLG ⇔ LL), occurs, with a break $P-T$ curve (or drop in heat capacity). A transition from two-phase (LL) equilibria to one-phase (L), (LL ⇔ L), takes place, at further isochoric heating of the mixture at high pressures.

2. At the highest average densities and low concentrations of *n*-pentane, before the thermal expansion causes the liquids to fill the entire volume, the initially immiscible liquid water + *n*-pentane mixture becomes miscible due to the positive temperature coefficient of solubility typical for water + *n*-alkane mixture. In this case, the first phase transition is the miscibility of *n*-pentane in water in equilibrium with its vapor, (LLG ⇔ LG), with a decrease in heat capacity as the number of phase decreases. In this case the isochoric $P-T$ break point is pronounced very slightly (very weak). On further heating of the two-phase (LG) mixture, the expanding liquid fills the entire cell, while the vapor phase disappears. A transition from two-phase (LG) to one-phase (L), (LG ⇔ L), takes place, with a break of the $P-T$ curves (decrease in heat capacity).

3. At the lowest average densities, heating increases the vapor density, resulting in disappearance of the liquid phases. A

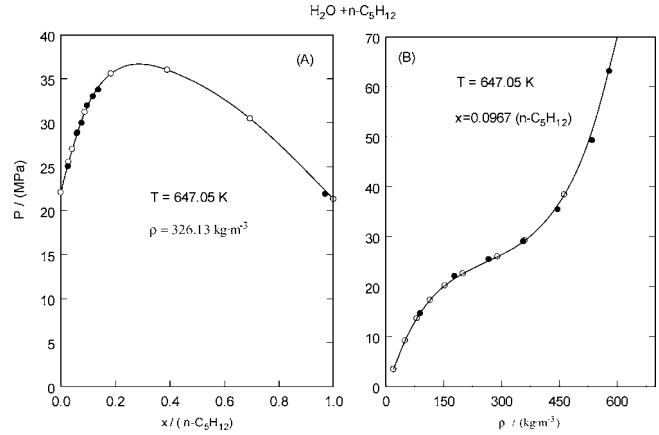

Figure 9. Comparison of the present measured pressures with the data reported by Abdulagatov et al.[12,13] along the selected near-critical isotherm (B) and isotherm-isochore (A). ●, this work; ○, Abdulagatov et al.;[14,15] —, smoothed experimental curves.

Table 3. Liquid−Gas P_S-T_S Phase Boundary Data for the H_2O + n-C_5H_{12} Mixtures Derived from the Break-Point Technique Using the Present *PVTx* Measurements

T_S/K	P_S/MPa	T_S/K	P_S/MPa
$x = 0.1380$ mole fraction of n-C_5H_{12}		$x = 0.0967$ mole fraction of n-C_5H_{12}	
569.20	8.880	567.15	7.700
573.83	11.200	577.15	10.902
590.69	14.334	582.82	12.614
597.39	17.315	590.20	14.547
604.31	18.051	599.51	17.115
615.26	23.354	624.82	29.411
623.17	30.922	626.47	40.470
629.30	44.413	633.15	54.715
635.82	61.255		
$x = 0.0270$ mole fraction of n-C_5H_{12}		$x = 0.1185$ mole fraction of n-C_5H_{12}	
606.15	13.315	564.56	8.836
629.52	19.014	573.47	10.801
634.78	21.501	592.88	13.912
637.17	23.092	606.83	17.574
635.73	23.854	612.56	20.247
630.31	25.912	619.08	24.000
625.52	27.718	622.57	30.066
622.05	37.634	628.49	43.900
$x = 0.075$ mole fraction of n-C_5H_{12}		$x = 0.058$ mole fraction of n-C_5H_{12}	
595.49	13.693	568.66	8.642
614.77	20.233	596.29	14.151
621.66	22.116	611.82	18.154
629.85	24.814	633.15	25.250
630.95	26.780	627.46	27.885
627.45	29.820	625.79	39.278
625.65	37.780	629.44	51.880
634.50	61.000		

Table 4. Measured Values of $P-T$ for the H_2O + n-C_5H_{12} Mixtures along the Three-Phase (LLG) Curve

T_{LLG}/K	P_{LLG}/MPa
412.55	1.704
438.22	2.775
449.63	3.544
460.35	4.352
463.85	4.575

transition takes place from three-phase (LLG) to two-phase equilibria (LG), (LLG ⇔ LG), again with a break of the $P-T$ curve (drop in the heat capacity). A transition from two-phase (LG) equilibria to one-phase (G), (LG ⇔ G), takes place, at further isochoric heating of the mixture with a break of the $P-T$ curve.

All of these cases have been encountered in our *PVTx* experiment for water−*n*-pentane mixture and in our previous

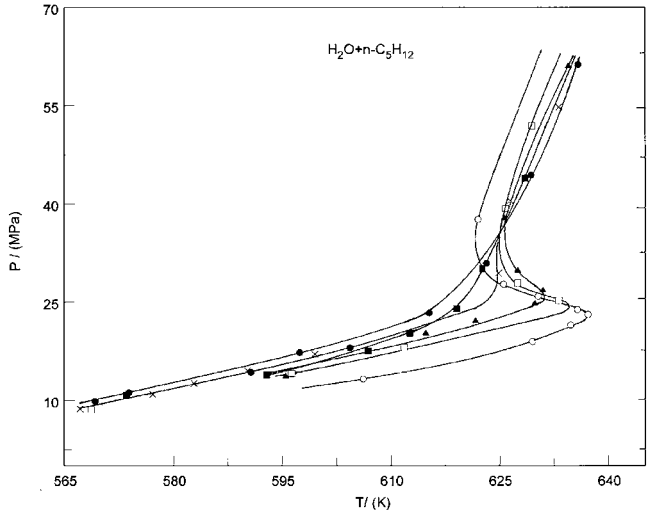

Figure 10. Upper P_S-T_S phase boundary curves of the $H_2O + n\text{-}C_5H_{12}$ mixtures. ●, $x = 0.8620$ mole fraction of water; ○, $x = 0.9730$ mole fraction of water; ▲, $x = 0.9250$ mole fraction of water; ×, $x = 0.9033$ mole fraction of water; ■, $x = 0.8815$ mole fraction of water; □, $x = 0.9420$ mole fraction of water. The solid curves are guides for the eye (smoothed curves).

PVTx and C_V experiments[35] for the water−*n*-hexane mixture. The first break point (or C_V jump) marks the disappearance of one of the liquid phases, and the second break (or C_V jump) marks the disappearance of the liquid or vapor phase depending on filling factor.

The filling factor (total density) is a very important for the experimentally observing of break points. For example, when approaching the critical isochore (see Figure 7), it is increasingly difficult to differentiate between the one- and the two-phase regions, while for the isotherms far from the critical region, the break points are very clearly pronounced. Near the critical point the transformation from the one- to two-phase (or from two- to one-phase) regions takes place without sharp changes (breaks) of the slopes of the isochores. Therefore, the isochoric $P-T$ break-point technique is much less sensitive to a phase transition in the critical region because the slopes of the $P-T$ curves change very little due to the small difference between the densities of the phases in equilibrium. Conversely, the quasi-static thermogram method[38,39] is more sensitive to determine the phase-boundary properties than the $P-T$ break-point technique, because in the critical region the isochoric heat capacity jump is very large (diverges as $\Delta C_V \propto (T - T_C)^{-\alpha}$, where $\alpha = 0.11$ is the universal critical exponent). At temperatures and pressures far from the critical point, the $P-T$ break-point technique is preferred because the heat-capacity jump ΔC_V is small (therefore, changes in thermogram slopes are also small), while the slopes of the $P-T$ isochores exhibit breaks that are sharp.

The isochore of 270 kg·m^{-3} for the concentration of $x = 0.791$ mole fraction of *n*-pentane intersects the phase-transition temperature at the UCEP ($T_{UCEP} = 463.85$ K and $P_{UCEP} = 4.575$ MPa), where the three-phase curve LLG intersects the lower L = G critical curve (see Figure 2). Figure 10 shows the (P_S,T_S) data at the LG phase boundary curve obtained on isochores entering the two-phase region. These data are also presented in Table 3. The qualitative comparison between the T_S-P_S data reported by de Loos et al.[6] (the reported data presented only graphically) and the present data for three selected concentrations is presented in Figure 11. As Figure 11 shows, in general, the agreement between the present results and the data reported by de Loos et al.[6] is satisfactory. We determined the phase-

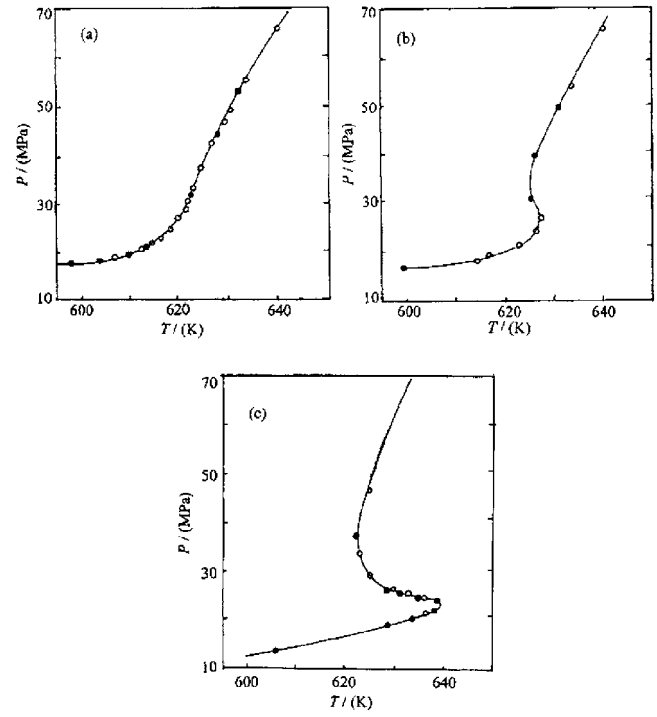

Figure 11. Comparison between the present derived values of liquid−gas phase boundary (T_S,P_S) data and the values reported by de Loos et al.[6] ●, this work; ○, de Loos et al.[6] (a) $x = 0.862$ mole fraction of water ($x = 0.859$, de Loos et al.[6]); (b) $x = 0.9033$ mole fraction of water ($x = 0.908$, de Loos et al.[6]); and (c) $x = 0.973$ mole fraction of water ($x = 0.967$, de Loos et al.[6]). The solid curves are guides for the eye (smoothed curves).

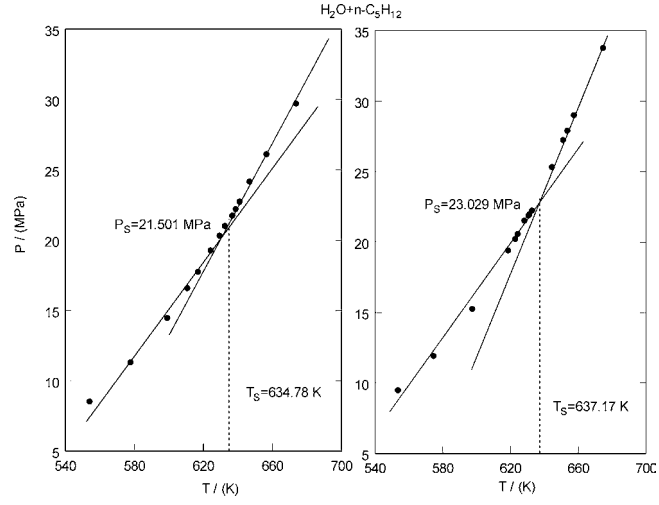

Figure 12. Intercept of the two- and one-phase $P-T$ (isochoric break points) for two selected isochores, $\rho = 282.60$ kg·m^{-3} (left) and $\rho = 376.87$ kg·m^{-3} (right) at a concentration of $x = 0.027$ mole fraction of *n*-pentane.

transition pressures and temperatures by "straight" extrapolations of the isochore behavior before and after phase transition occurs. The phase-transition points were determined as the intersection of the three-, two-, and one-phase $P-T$ curves. Figures 12 and 13 show examples of liquid and vapor one-phase, two-phase, and three-phase $P-T$ data along the three selected isochores for two concentrations of 0.027 and 0.8898 mole fraction of *n*-pentane. These figures show a detailed (expanded) view of the $P-T$ curve behavior in the various regions of the phase diagram.

The same procedure was applied for the lower branch of the two-phase (LG) T_S-P_S phase boundary and three-phase (LLG) curves. Figure 14 shows lower liquid−gas phase boundary

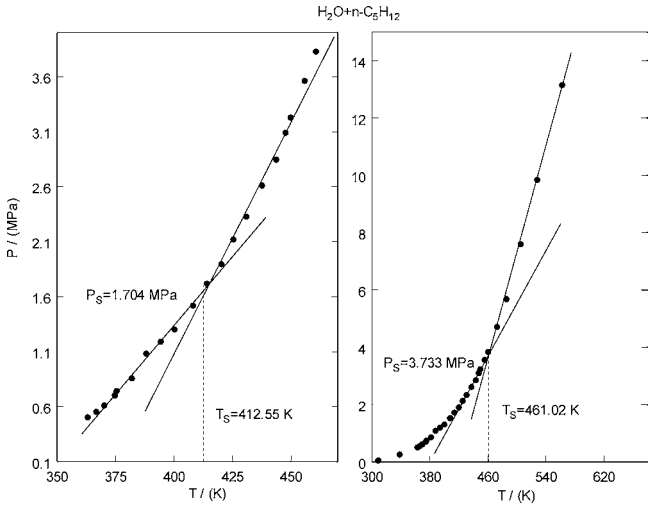

Figure 13. Intercept of the three- and two-phase (left) and two- and one-phase (right) $P-T$ isochore, $\rho = 316.5$ kg·m^{-3} (isochoric break points) for the selected concentration $x = 0.8898$ mole fraction of *n*-pentane.

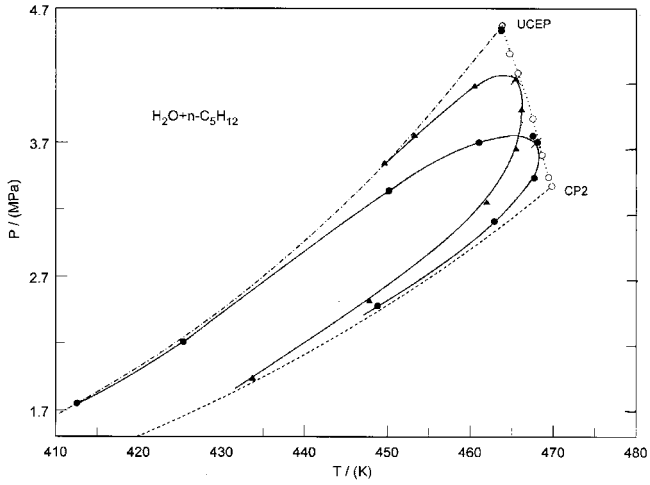

Figure 14. Three- and two-phase $P-T$ phase boundary curves for the $H_2O + n$-C_5H_{12} mixtures at two selected concentrations. ●, $x = 0.8898$; ▲, $x = 0.8260$; ×, lower critical points for these concentrations (this work); ○, lower critical point data;[7] —, experimental smoothed liquid−gas phase boundary curve (this work); -·-·-·-, three-phase (LLG) curve;[17] ----, vapor-pressure curve of pure *n*-C_5H_{12} (Span and Wagner[48]); CP2, critical point of *n*-C_5H_{12}; UCEP, upper critical end point (this work).

curves for the $H_2O + C_5H_{12}$ mixture together with the three-phase curve derived from the present *PVTx* measurements using the break-point technique. The derived values of T_S and P_S have an uncertainty of about (0.2 to 0.5) K and (0.1 to 0.2) MPa in the range far from the critical point and (1 to 2) K and (0.5 to 1.0) MPa in the critical region, where the location of the break points is unclear, respectively. Because the values of the phase-transition temperatures (T_S) and pressures (P_S) were obtained by graphical−analytical methods as isochoric break points, these data have relatively large uncertainties in comparison with the methods of direct measurements. The uncertainty of the interpolating procedure far from the critical region is negligibly small since the experimental $P-T$ and $P-x$ curves are very simple (almost linear) and can be reproduced analytically with high accuracy.

Critical Curve Data and the Krichevskii Parameter. Using the two-phase T_S-P_S phase boundary data, the values of the critical properties of the binary $H_2O + n$-C_5H_{12} mixtures were derived. The derived values of the critical parameters of upper and lower critical curves are presented in Table 5 and 6 and shown in Figures 3 and 4 in the T_C-P_C, T_C-x, and P_C-x projections together with the reported data. As one can see from these figures, the derived critical temperatures and pressures are in fair agreement with the data reported by other authors. The present result is in satisfactory agreement with the interpolated values calculated from the data by de Loos et al.[6] and Brunner.[7] For example, the derived values of the critical pressure ($P_C = 75.50$ MPa) and the critical temperature ($T_C = 646.30$ K) for the concentration of $x = 0.115$ mole fraction of *n*-C_5H_{12} are in satisfactory (within 1.4 MPa and 0.4 K) agreement with the values 76.90 MPa and 646.7 K, reported by de Loos et al.[6] for very close (0.118 mole fraction) to the present concentration. Figure 9 shows the present $P-x$ data for the concentration dependence of the measured pressures along the critical isotherm−isochore of pure water together with the previous reported data by Abdulagatov et al.[14,15] As one can see, the initial slope of the $P-x$ curve ($x \rightarrow 0$, the Krichevskii parameter), derived from the present and reported data, at 139.03 MPa, is in satisfactory agreement with the value of 158.0 MPa derived by Abdulagatov et al.[40] from the critical curve data. The Krichevskii parameter for this mixture also was reported previously by several authors: Plyasunov and Shock[41] (181 ± 30 MPa), Plyasunov and Shock[42] (168 MPa), and Abdulagatov et al.[43] (198 ± 40 MPa) using the critical properties data. Krichevskii[44] derived the relation between the initial slopes of the critical lines and the derivative $(\partial P/\partial x)^{\infty}_{T_C V_C}$

$$\left(\frac{\partial P}{\partial x}\right)^{C}_{V_C T_C} = \left[\left(\frac{dP_c}{dT_c}\right)^{C}_{CRL} - \left(\frac{dP_S}{dT}\right)^{C}_{CXC}\right]\left(\frac{dT_c}{dx}\right)^{C}_{CRL} \qquad (4)$$

where "$_{CXC}$" and "$_{CRL}$" subscripts are related to the vapor-pressure and critical line curves, respectively. The regimes of the near-critical dilute solution behavior depend strongly on the signs and magnitudes of the initial slopes of the critical curves of $T_C(x)$ and $P_C(x)$ and on the slope of the vapor-pressure curve $(dP_S/dT)^{C}_{CXC}$ at the critical point of the pure solvent (water), that is, the magnitude and sign of the Krichevskii parameter, $(\partial P/\partial x)^{C}_{T_C V_C}$.[45] The value of the derivative $(dP_S/dT)^{C}_{CXC} = 0.2682$ MPa·K^{-1} for pure water is calculated with the vapor-pressure equation (IAPWS formulation, Levelt-Sengers[46]), and the slopes of the critical curves $T_C(x)$ and T_C-P_C are from the measured and reported data. The value of $(dP_C/dT_C)_{CRL} = -0.0406$ MPa·K^{-1} for $H_2O + n$-C_5H_{12} at the critical point of pure water is lower than the value of the vapor-pressure curve $(dP_S/dT)^{C}_{CXC}$ for water at the critical point (see Figure 3). Therefore, as one can see from eq 4, the value of the Krichevskii parameter of $H_2O + n$-C_5H_{12} is positive because the value of the derivative

Table 5. Upper Critical Curve of the $H_2O + n$-C_5H_{12} Mixtures Derived from the Present *PVTx* Measurements

x/mole fraction of *n*-C_5H_{12}	T_C/K	P_C/MPa
0.1185	646.30	75.50
0.0967	629.95	49.70
0.0750	625.50	33.90
0.0580	627.05	27.10
0.0270	632.35	21.78
0.0000	647.10	22.15

Table 6. Lower Critical Curve of the $H_2O + n$-C_5H_{12} Mixtures Derived from the Present *PVTx* Measurements

x/mole fraction of *n*-C_5H_{12}	T_C/K	P_C/MPa
1.0000	469.90	3.36
0.8898	467.93	3.70
0.8570	466.68	3.90
0.8260	465.45	4.17
0.7970	464.15	4.50
0.7910	463.85	4.57

$(dT_C/dx)_{CRL} < 0$ is negative. The value of the derivative $(dT_C/dx)_{x=0} = -466.67$ K at infinite dilution ($x \rightarrow 0$) calculated from the present and the reported data were used to determine the value of the Krichevskii parameter for the $H_2O + n\text{-}C_5H_{12}$ mixture. Our result for the Krichevskii parameter calculated with eq 4 is (144.11 ± 5) MPa. This means that when exchanging a solvent (water) molecule by one solute ($n\text{-}C_5H_{12}$) molecule at constant volume and temperature, the local density of water molecules around the $n\text{-}C_5H_{12}$ molecule is decreasing compared with the ideal mixture or bulk density of pure water. Therefore, a dilute $H_2O + n\text{-}C_5H_{12}$ mixture is a "repulsive" mixture according to the classification by Levelt-Sengers[45] and Debenedetti and Mohamed.[47] The value of the Krichevskii parameter derived from the present and reported critical curve data (144.11 MPa) is excellent agreement with the value (139.03 MPa) derived from the direct $P-x$ measurements along the critical isochore−isotherm of pure water.

Conclusions

New measurements of the *PVTx* properties of the $H_2O + n\text{-}C_5H_{12}$ mixtures were reported along 66 liquid and vapor isochores from (63 to 713) kg·m^{-3} as a function of temperature in the range from (303 to 684) K at pressures up to 63 MPa. These regions include upper and lower branches of the critical curves, the three-phase line, and LG, LL, and GG phase equilibrium curves. The measured data were used to determine the values of the three-phase (LLG) and two-phase (LG) phase boundary properties (T_S,P_S) and the critical parameters (T_C,P_C) of the $H_2O + n\text{-}C_5H_{12}$ mixtures. The values of the upper critical point parameters ($T_{UCEP} = 463.85$ K, $P_{UCEP} = 4.575$ MPa, and the concentration $x = 0.791$ mole fraction of *n*-pentane) are derived from the three-phase (LLG) curve data. The value of the Krichevskii parameter calculated using the critical line data (144.11 ± 5 MPa) and the direct $P-x$ data along the critical isochore−isotherm of pure water (139.03 MPa) was obtained.

Acknowledgment

I.M.A. thanks the Thermophysical Properties Division at the National Institute of Standards and Technology for the opportunity to work as a Guest Researcher at NIST during the course of this research.

Literature Cited

(1) Morrow, N. M. *Interface Phenomena in Petroleum Recovery*; Dekker: New York, 1991; p 1.
(2) Siskin, M.; Katritzky, A. R. Reactivity of organic compounds in hot water: geological and technological implications. *Science* **1991**, *254*, 231–237.
(3) Weingaertner, H.; Franck, E. U. Supercritical water. *Angew. Chem., Int. Ed.* **2005**, *44*, 2672–2692.
(4) O'Brien, C. P.; Theis, M. C.; Bruce, D. A. Supercritical water oxidation of the PCB congener 2-chlorobiphenil in methanol solutions: a kinetic analysis. *Environ. Sci. Technol.* **2005**, *39*, 6839–6844.
(5) Eckert, C. A.; Liotta, C. L.; Bush, D.; Brown, J. S.; Hallett, J. P. Sustainable reactions in tunable solvents. *J. Phys. Chem.* **2004**, *108*, 18108–180118.
(6) de Loos, T. W.; van Dorp, J. H.; Lichtenthaler, R. N. Phase equilibria and critical phenomena in fluid (*n*-alkane + water) systems at high pressures and temperatures. *Fluid Phase Equilib.* **1983**, *10*, 279–287.
(7) Brunner, E. Fluid mixtures at high pressures. IX. Phase separation and critical phenomena in 23 (*n*-alkane + water) mixtures. *J. Chem. Thermodyn.* **1990**, *22*, 335–353.
(8) Connolly, J. F. Solubility of hydrocarbons in water near the critical temperature. *J. Chem. Eng. Data* **1966**, *11*, 13–17.
(9) Roof, J. G. Three-phase critical point in hydrocarbon + water systems. *J. Chem. Eng. Data* **1970**, *15*, 301–303.
(10) Anisimov, M. A.; Sengers, J. V. Critical region. In *Equations of State for Fluids and Fluids Mixtures*; Sengers, J. V., Kayser, R. F., Peters, C. J., White, H. J., Eds.; Elsevier: Amsterdam, 2000; pp 381−434.
(11) Fisher, M. E. Renormalization of the critical exponents by hidden variables. *Phys. Rev. B* **1968**, *176*, 257–271.
(12) de Loos, T. W.; Wijen, A. J. M.; Diepen, G. A. M. Phase equilibria and critical phenomena in fluid (propane + water) at high pressures and temperatures. *J. Chem. Thermodyn.* **1980**, *12*, 193–204.
(13) Neichel, M.; Franck, E. U. Critical curves and phase equilibria of water-*n*-alkane binary systems to high pressures and temperatures. *J. Supercrit. Fluids* **1996**, *9*, 69–74.
(14) Abdulagatov, I. M.; Bazaev, A. R.; Bazaev, E. A.; Saidakhmedova, M. B.; Ramazanova, A. E. Excess, partial, and apparent molar volumes of *n*-alkanes in near- and supercritical water. *J. Solution Chem.* **1998**, *27*, 731–753.
(15) Abdulagatov, I. M.; Bazaev, A. R.; Bazaev, E. A.; Saidakhmedova, M. B.; Ramazanova, A. E. Volumetric properties of near- and supercritical water-*n*-pentane mixtures: Molar, excess, partial, and apparent volumes. *J. Chem. Eng. Data* **1998**, *43*, 451–458.
(16) Scheffer, F. E. On mixing in a binary system for which the three phase pressure is greater than the sum of the vapor tensions of the two components. *Proc. Sect. Sci.* **1914**, *17*, 834–839.
(17) Jou, F. Y.; Mather, A. E. Vapor-liquid-liquid locus of the system pentane + water. *J. Chem. Eng. Data* **2000**, *45*, 728–729.
(18) Gillespie, P. C.; Wilson, G. M. *Vapor-liquid and liquid-liquid equilibria: Water-methane, water-carbon dioxide, water-hydrogen sulfide, water-n-pentane, water-methane-n-pentane*; Gas Processors Association Research Report RR-48, Project 758-B-77 for Wiltec Res. Co., Inc.: Provo, UT, 1982.
(19) Wormald, C. J.; Colling, C. N.; Lancaste, N. M.; Sellers, A. J. *Excess enthalpy experimental data. Binary mixtures: Water + n-pentane; Water + n-hexane; Water + n-heptane, and Water + n-octane*; Research Report, RR-68, University of Bristol, Bristol, U.K., 1983.
(20) Rasulov, S. M. *PVT* properties and phase equilibrium in binary water + *n*-pentane mixture. *Russ. J. Phys. Chem.* **2009**, *83*, 756–759.
(21) Kamilov, I. K.; Stepanov, G. V.; Rasulov, S. M. Liquid-liquid and liquid-gas equilibrium curves and critical lines of water + *n*-hexane mixture. *High Temp. High Pressures* **1997**, *29*, 491–495.
(22) Rasulov, S. M.; Isaev, I. A. Phase equilibrium and the critical lines in water + *n*-pentane and water + *n*-hexane mixtures. *Russ. High Temp.* **2006**, *44*, 847–859.
(23) Rasulov, S. M.; Rasulov, A. R. Liquid-liquid equilibria and *PVT* properties of binary water-*n*-hexane mixtures. *Russ. J. Phys. Chem.* **2000**, *74*, 1613–1615.
(24) Rasulov, S. M.; Rasulov, A. P. *PVT*-dependence of the water + *n*-octane-sodium dodecylsulfate microemulsion + *n*-pentanol for two compositions. *Russ. High Temp.* **2008**, *46*, 953–956.
(25) Rasulov, A. R.; Rasulov, S. M.; Radzhabova, L. M. In *Thermal properties of n-butanol in the near-critical region*, Proc. 12th Russian Thermophys. Prop. Conf., Moscow, 2008; pp 286−289.
(26) Wagner, W.; Pruss, A. The IAPWS formulation 1995 for the thermodynamic properties of ordinary water substance for general and scientific use. *J. Phys. Chem. Ref. Data* **2002**, *31*, 387–535.
(27) Mather, A. E.; Sadus, R. J.; Franck, E. U. Phase equilibria in (water + krypton) at pressures from 31 to 273 MPa and temperatures from 610 to 660 K and in (water + neon) from 45 to 255 MPa and from 660 to 700 K. *J. Chem. Thermodyn.* **1993**, *25*, 771–779.
(28) Shmonov, V. M.; Sadus, R. J.; Franck, E. U. High-pressure phase equilibria and supercritical *pVT* data of the binary water + methane mixture to 723 K and 200 MPa. *J. Phys. Chem.* **1993**, *97*, 9054–9059.
(29) Lentz, H. A method of studying the behavior of fluid phases at high pressures and temperatures. *Rev. Sci. Instrum.* **1968**, *40*, 371–372.
(30) Levelt-Sengers, J. M. H.; Hastings, J. R. Equation of state of ethylene vapor between 223 and 273 K by the Burnett method. *Int. J. Thermophys.* **1981**, *2*, 269–288.
(31) Bazaev, A. R.; Abdulagatov, I. M.; Bazaev, E. A.; Abdurashidova, A. A.; Ramazanova, A. E. *PVT* measurements for pure methanol in the near-critical and supercritical regions. *J. Supercrit. Fluids* **2007**, *41*, 217–226.
(32) Bach, R. W.; Friedrichs, H. A. *p-V-T* relations for HCl-H_2O mixtures up to 500 °C and 1500 bar. *High Temp. High Pressures* **1977**, *9*, 305–312.
(33) Bazaev, A. R.; Abdulagatov, I. M.; Magee, J. W.; Bazaev, E. A.; Ramazanova, A. E.; Abdurashidova, A. *PVTx* measurements for a H_2O + methanol mixture in the sub-critical and supercritical regions. *Int. J. Thermophys.* **2004**, *25*, 804–838.
(34) Polikhronidi, N. G.; Abdulagtaov, I. M.; Batyrova, R. G.; Stepanov, G. V. Experimental study of the *PVTx* properties of aqueous ammonia mixture in the critical and supercritical regions. *Int. J. Refrig.* **2009**, *32*, 1897–1913.
(35) Kamilov, I. K.; Stepanov, G. V.; Abdulagatov, I. M.; Rasulov, A. R.; Milikhina, E. M. Liquid-liquid-vapor and liquid-vapor phase transitions in aqueous *n*-hexane mixtures from isochoric heat capacity measurements. *J. Chem. Eng. Data* **2001**, *46*, 1556–1567.
(36) Kamilov, I. K.; Stepanov, G. V.; Malysheva, L. V.; Rasulov, A. R.; Rasulov, S. M.; Shakhbanov, K. A. Phase equilibrium curves and

critical lines of *n*-hexane-water: liquid-liquid and liquid-gas. *High Temp. High Pressures* **1997**, *29*, 237–246.
(37) Polikhronidi, N. G.; Stepanov, G. V.; Abdulagatov, I. M.; Batyrova, R. G. Thermodynamic study of the *n*-octane-1-pentanol-sodium dodecyl sulfate solutions in water. *Thermochim. Acta* **2007**, *454*, 99–108.
(38) Abdulagatov, I. M.; Polikhronidi, N. G.; Bruno, T. J.; Batyrova, R. G.; Stepanov, G. V. Measurements of the isochoric heat capacity, the critical point (T_C, ρ_C) and vapor−liquid coexistence curve (T_S, ρ_S) of high-purity toluene near the critical point. *Fluid Phase Equilib.* **2008**, *263*, 71–84.
(39) Polikhronidi, N. G.; Abdulagatov, I. M.; Batyrova, R. G. Features of isochoric heat capacity measurements near the phase transition points. *Fluid Phase Equilib.* **2002**, *201*, 269–286.
(40) Abdulagatov, A. I.; Stepanov, G. V.; Abdulagatov, I. M. Krichevskii parameter and thermodynamic properties infinite dilute aqueous solutions near the critical point of pure water. *Russ. Supercrit. Fluids Theory Pract.* **2007**, *2*, 20–54.
(41) Plyasunov, A. V.; Shock, E. L. Estimation of the Krichevskii parameter for aqueous nonelectrolytes. *J. Supercrit. Fluids* **2001**, *20*, 91–103.
(42) Plyasunov, A. V.; Shock, E. L. Prediction of the vapor-liquid distribution constants for volatile nonelectrolytes in water up to its critical temperature. *Geochim. Cosmochim. Acta* **2003**, *67*, 4981–5009.
(43) Abdulagatov, A. I.; Stepanov, G. V.; Abdulagatov, I. M. Crossover equation of state and microstructure properties of infinite dilute solutions near the critical point of pure solvent. *Russ. J. Struct. Chem.* **2001**, *48*, 585–597.
(44) Krichevskii, I. R. Thermodynamics of critical phenomena in infinitely dilute binary solutions. *Russ. J. Phys. Chem.* **1967**, *41*, 1332–1338.
(45) Levelt Sengers, J. M. H. Solubility near the sovent's critical point. *J. Supercrit. Fluids* **1991**, *4*, 215–222.
(46) Levelt-Sengers, J. M. H. Saturated properties of ordinary water substance. In *Physical Chemistry of Aqueous Systems*, Proceedings of the 12th International Conference Properties of Water and Steam, Begell House, NY, 1995; White, H. J., Sengers, J. V., Neumann, D. B., Bellows, J. C., Eds.; pp A143−149.
(47) Debenedetti, P. G.; Mohamed, R. S. Attractive, weakly attractive and repulsive near-critical systems. *J. Chem. Phys.* **1989**, *90*, 4528.
(48) Span, R.; Wagner, W. Equation of state for technical applications. II. Results for Nonpolar Fluids. *Int. J. Thermophys.* **2003**, *24*, 41–109.

Received for review January 21, 2010. Accepted April 28, 2010.

JE100073Y